



Universiteit
Leiden
The Netherlands

In vivo high field magnetic resonance imaging and spectroscopy of adult zebrafish

Kabli, S.

Citation

Kabli, S. (2009, October 7). *In vivo high field magnetic resonance imaging and spectroscopy of adult zebrafish*. Retrieved from <https://hdl.handle.net/1887/14040>

Version: Corrected Publisher's Version

License: [Licence agreement concerning inclusion of doctoral thesis in the Institutional Repository of the University of Leiden](#)

Downloaded from: <https://hdl.handle.net/1887/14040>

Note: To cite this publication please use the final published version (if applicable).

***In Vivo* High Field Magnetic
Resonance Imaging and
Spectroscopy of Adult Zebrafish**

Samira Kabli

ISBN: 978-90-9024529-4

***In Vivo* High Field Magnetic Resonance
Imaging and Spectroscopy of Adult Zebrafish**

Proefschrift

ter verkrijging van
de graad van Doctor aan de Universiteit Leiden,
op gezag van Rector Magnificus prof.mr. P.F. van der Heijden,
volgens besluit van het College voor Promoties
te verdedigen op 7 oktober 2009
klokke 15.00 uur

door

Samira Kabli

geboren te Amsterdam, in 27 September 1974

Promotiecommissie:

Promotor:

Prof. dr. H.J.M. de Groot

Copromotor:

Dr. A. Alia

Overige leden:

Prof. dr. J. Brouwer

Prof. dr. J.P. Abrahams

Prof. dr. H.P. Spaink

Dr. D. Gross

Voor mijn ouders

Contents

List of abbreviations	12
1 General introduction	15
1.1 Zebrafish as a model for Cancer	16
1.2 Zebrafish as a model for studying brain disorders	18
1.3 MRI theoretical background	20
1.3.1 Rapid acquisition with relaxation-enhancement imaging	26
1.3.2 Transverse relaxation mapping	27
1.4 Magnetic resonance spectroscopy	28
1.5 MRI/MRS at ultra-high magnetic field	31
1.6 Scope of the thesis	32
References	34
2 Magnetic Resonance Microimaging of the Adult Zebrafish	41
2.1 Abstract	41
2.2 Introduction	42
2.3 Materials and methods	44
2.4 Results	46
2.4.1 <i>Ex vivo</i> studies	47
2.4.2 <i>In vivo</i> studies	51
2.4.3 Three-dimensional image reconstruction	53

2.5	Discussion	55
	Acknowledgements	56
	References	56
3	<i>In Vivo</i> Metabolite Profile of Adult Zebrafish Brain Obtained by High Resolution Localized Magnetic Resonance Spectroscopy	61
3.1	Abstract	61
3.2	Introduction	62
3.3	Materials and methods	64
3.4	Results	68
3.4.1	<i>In vivo</i> proton MR spectroscopy of adult zebrafish brain	68
3.4.2	<i>In vitro</i> proton NMR spectroscopy of the zebrafish brain extracts	71
3.5	Discussion	75
	Acknowledgements	77
	References	78
4	<i>In Vivo</i> Ultra High Field Magnetic Resonance Microimaging to Monitor Malignant Melanoma in Zebrafish	81
4.1	Abstract	81
4.2	Introduction	82
4.3	Materials and methods	84
4.4	Results and discussion	86
	Acknowledgements	94

References	94
5 General discussion and future outlook	97
5.1 Future perspectives of MR imaging of the adult zebrafish	97
5.2 High resolution localized MR spectroscopy of adult zebrafish brain and future perspective	101
5.3 Monitoring spontaneous melanomas in transgenic zebrafish with μ MRI and beyond	103
References	104
Summary	108
Samenvatting	111
Curriculum Vitae	114
List of publications	116
Nawoord	119

List of abbreviations

μ MRI	Magnetic Resonance micro-Imaging
1D	One-dimensional
2D	Two-dimensional
3D	Three-dimensional
Ala	Alanine
Asp	Aspartate
ATP	Adenosine-5'-triphosphate
ADP	Adenosine diphosphate
Cho	Choline
COSY	Correlation Spectroscopy
CNR	Contrast-to-Noise Ratio
Cr	Creatine
EDTA	Ethylenediaminetetraacetic acid
FASTMAP	Automatic shimming method
FID	Free induction decay
fMRI	Functional Magnetic Resonance Imaging
FOV	Field of View
FSE	Fast Spin Echo
GABA	γ -Aminobutyric acid
GE	Gradient Echo
GFP	Green fluorescent protein
Glc	Glucose

Gln	Glutamine
Glu	Glutamate
Glx	Glutamine + Glutamate
GPC	Glycerophosphocholine
Gro	Glycerol
GSH	Glutathione
HCar	Homocarnosine
HRas	Human Ras
Ins	Inositol
IR-RARE	Inversion Recovery RARE
Lac	Lactate
mI	<i>myo</i> -Inositol
mitf	Mammalian microphthalmia-associated transcription factor
MPTP	methyl-4-phenyl- 1,2,3,6- tetrahydropyridine
MRA	Magnetic Resonance Angiography
MRI	Magnetic Resonance Imaging
MRS	Magnetic Resonance Spectroscopy
MS222	Ethyl meta aminobenzoate metanesulfonic acid salt
MSME	Multi-Slice Multi-Echo
MTX	Matrix
NA	Number of Averages
NAA	N-Acetylaspartate
NAAG	N-acetylaspartylglutamate
NEX	Number of Excitations
NMR	Nuclear Magnetic Resonance
OVS	Outer Volume Suppression

PCh	Phosphocholine
PCr	Phosphocreatine
PE	Phosphoethanolamine
P _i	Inorganic Phosphate
PRESS	Point REsolved SpectroScopy
PS1, PS2	Presenilin 1, Presenilin 2
P53	53 kDa tumor protein, which suppresses tumor growth
RARE	Rapid Acquisition with Relaxation Enhancement
RAS	A protein which regulates the oncogenic pathways
RF	Radio frequency
RNA	Ribonucleic acid
ROI	Region Of Interest
SE	Spin Echo
sI	<i>scyllo</i> -Inositol
SNR	Signal-to-Noise Ratio
T	Tesla
T ₁	Longitudinal or spin-lattice relaxation time
T ₂	Transverse or spin-spin relaxation time
Tau	Taurine
tCr	Total Creatine (Creatine + Phosphocreatine)
TE	Echo Time
Thr	Threonine
TR	Repetition Time
TSP	2,2,3,3-tetradeutero-3-trimethylsilylpropionic acid
Tyr	Tyrosine
VAPOR	Variable Pulse power and Optimized Relaxation delays
VOI	Volume Of Interest

1 General introduction

Biomedical research depends on the use of animal models to understand the pathogenesis of human disease at the cellular and molecular level and to provide systems for developing and testing new therapies. Mammalian models, such as the mouse, have been pre-eminent in modeling human diseases, primarily because of the striking homology between mammalian genomes and the many similarities in the biology of mice and human beings, spanning from anatomy to cell biology and physiology. Despite the pre-eminence of the mouse in modeling human disease, several aspects of murine biology have limited its routine use in large-scale genetic and therapeutic screening. For example, although forward-genetic screens (1-4) and randommutagenesis-based reverse genetics (5, 6) are feasible in the mouse and are currently underway, they cannot be applied routinely on the desired scale because they require considerable staff and infrastructure support. Hence, such approaches in mice are limited to a few large projects, often operating as screening consortia. In this context, the zebrafish (*Danio rerio*) has emerged recently as a versatile and genetically tractable alternative vertebrate model system. Sophisticated mutagenesis and screening strategies on a large scale, and with an economy that is not possible in other vertebrate systems, have generated zebrafish models of a wide variety of human diseases.

The zebrafish has also proven to be a useful and relevant model for studying vertebrate development and organogenesis (7, 8). It exhibits high fecundity,

about 200 eggs per week per female. Embryos develop rapidly in fresh water externally to the mother and are therefore easily manipulated *ex utero*, while progressing from fertilized eggs to free swimming larvae in 60 h. In addition, zebrafish embryos are transparent. Visualization of all stages of organ development is relatively easy in the first few days of life when the fish is only a few millimetres in length, and this can be combined with manipulation of gene expression at RNA and protein levels. Gene expression can be induced using microinjection of specific vectors at very early stages and is generally highly effective for at least the first 2 days of development (9). Because it can easily take up chemicals from water, zebrafish is also used as a pharmacological tool in drug discovery and ecotoxicity research (10-12). As it can live in as little as a few microlitres of fluid, only micrograms of compound per assay are needed for screening. This facilitates screening of compounds, enabling *in vivo* analysis of compound action at much earlier stages and higher throughput than hitherto possible. Clearly, the zebrafish model combines the relevance of a vertebrate with the scalability of an invertebrate and, in many studies, could provide an interesting intermediate vertebrate model to laboratory small mammals.

1.1 Zebrafish as a model for Cancer

In recent years, zebrafish received strong attention from cancer researchers, after it was discovered that zebrafish can develop almost any type of cancer (13). A critical asset of zebrafish as a cancer model is that many tumors histologically resemble human tumors (14). In addition, more general cancer characteristics such as genomic instability, invasiveness, transplantability, and the existence of cancer stem cells (15) apply to zebrafish tumors as well,

and many tumor suppressor genes and oncogenes have been conserved. Further, the development of fish lines harboring oncogenic transgenes and their amenability to genetic and pharmacological testing also made zebrafish a favorable model. Cancer progression in zebrafish recapitulates many aspects of human disease and opens the door for studies to identify genetic and chemical modifiers of cancer (14, 16-20). The development of xenograft models allow the propagation and visualization of human cancer cells engrafted in optically transparent zebrafish (21-25). Numerous mutant or tissue-specific transgenic cancer fish lines are available (14, 16-20). Zebrafish can also efficiently absorb anticancer agents directly from water which makes this organism appealing for screening these compounds (20, 26). Taken together, these studies validate zebrafish as a *bona fide* cancer model.

Advanced melanoma is a devastating and lethal cancer (27). Melanoma arises from melanocytes, which are the pigment producing cells of human skin. Melanocytes can proliferate and give rise to various types of benign nevi, which are commonly referred to as moles. Transformed melanocytes can yield melanomas that initially grow radially in the epidermis. This is followed by the transition to a vertical growth phase that involves invasion through the basement membrane into the underlying dermis, preceding metastasis.

There are many areas of melanoma biology that are underexplored. For example, the steps by which a normal melanocyte becomes or generates a melanoma cell are largely unknown. How the disease subverts properties of normal melanocytes and their neural crest progenitors has been a topic of recent investigations, and this will be a fertile area of research in the future.

Lastly, while great progress has been made in identifying genetic defects that contribute to melanoma (28), there are clearly many more genes that remain to be tied to this disease. And significant challenges in the clinical management of this disease remain. These challenges are reflected in a very poor overall prognosis for patients with advanced melanoma, largely because there is no non-invasive early diagnosis and no effective therapy. (29). Translational research that uses fundamental knowledge of a disease to develop diagnostic and therapeutic strategies holds promise for improving melanoma treatment. The zebrafish melanoma model has unique attributes that may lead to important insights at the interface of melanocyte biology and clinical medicine.

1.2 Zebrafish as a model for studying brain disorders

Due to similar basic organization of brain components as that of human, zebrafish is increasingly used as a model for studying brain disorders (30-34). However, till now, modelling a brain disease in zebrafish requires optically transparent embryonic or larval, rather than adult, stages for optical detection that allows real-time imaging of developing pathologies. Experimentation with adult animals is not possible with optical methods, while diseases like neurodegeneration occur mainly at later stages in life. Considerable knowledge concerning the embryonic development of the central nervous system of the zebrafish has been collected in recent years. In contrast, there is an apparent lack of information on the organization of the adult zebrafish brain (35).

The zebrafish brain aminergic systems share many structural properties with the mammalian systems and practically all important physiological systems

in the brain involve the modulatory aminergic neurotransmitters. Many of these are also involved in human central nervous system diseases, including Parkinson's disease, schizophrenia, Alzheimer's disease, and depression. The noradrenergic, serotonergic, and histaminergic systems are highly similar (30-34). The dopaminergic systems also show similarities with the major difference being a lack of dopaminergic neurons in zebrafish mesencephalon. Development of automated quantitative behavioral analysis methods for zebrafish and imaging systems of complete brain neurotransmitter networks have enabled comprehensive studies on these systems in normal and pathological conditions at early developmental stages. Alterations of brain dopaminergic systems with neurotoxin such as MPTP, that in humans and rodents induces Parkinson's disease, induces both changes in the zebrafish dopaminergic system and quantifiable abnormalities in motor behavior (32). Chemically-induced brain histamine deficiency causes an identifiable alteration in histaminergic neurons and terminal networks, and a clear change in swimming behavior and long-term memory. Combining the imaging techniques and behavioral methods with zebrafish genetics is likely to help reveal how the modulatory transmitter systems interact to produce distinct behaviors, and how they are regulated in pathophysiological conditions and diseases. Several transgenic zebrafish models for neurodegeneration, such as Parkinson disease (30, 34), Huntington disease (36) and Alzheimer's disease (33) have been developed in recent years. However, imaging adult zebrafish brain *in vivo* was not feasible.

MRI is an imaging technique that can provide access to adult zebrafish brain anatomy with good resolution. It has been applied at embryonic stages, but not yet in adult fish. In addition, MRI in conjunction with MRS can be

invaluable for studying disease at molecular levels. In the following paragraph, a brief introduction of MRI and MRS and its relevance to zebrafish imaging and spectroscopy is presented.

1.3 MRI theoretical background

Magnetic resonance imaging (MRI) is a well-established non-invasive, diagnostic medical imaging technique based on the nuclear magnetic resonance (NMR) phenomenon (37). Every tissue in the body has a specific chemical makeup and thus the strength of the hydrogen NMR response differs from tissue to tissue. MRI allows the anatomy inside the body to be seen in either tomographic images taken along at any angle through the body, or three-dimensional volume images. The NMR information present in each pixel of one of these images is both temporal and spectral in nature. Conventional MRI relies on differences in a weighted average of the spectral and temporal information collected from different species to facilitate the diagnosis of diseases.

MR is based upon the interaction between an applied magnetic field and a nucleus with a nuclear magnetic moment or “spin” (37-39). Several nuclei, including ^1H , ^{31}P , ^{13}C , ^{15}N , and ^{19}F have nuclear magnetic moments corresponding with spin $\frac{1}{2}$ and are most suitable for detection by magnetic resonance (38-40). Protons are the most abundant spin $\frac{1}{2}$ nuclei in living organisms and they have the best NMR sensitivity (38-40). For this reason protons are the most frequently studied nuclei. As a crude simplification, nuclear spins can be thought of as small magnets. When placed in an external magnetic field (B_0) a large number of proton spins will be aligned parallel to B_0 , with a somewhat smaller number oriented anti-parallel. This

orientation yields a net nuclear magnetization and a net magnetization vector M_z parallel to B_0 .

After the RF pulse is switched off, the net magnetization vector will start reverting back to its equilibrium state as a result of a process which is called relaxation. The recovery process along the longitudinal axis is called T_1 relaxation, spin-lattice relaxation or longitudinal relaxation (Fig. 1A) and is described as:

$$M_z(t) = M_{z_{\max}} \left(1 - e^{-\frac{t}{T_1}}\right) \quad (1.1)$$

During a T_1 process, the nuclei are giving up energy to their immediate surroundings.

The dephasing process in the transverse plane (the plane orthogonal to B_0) is referred to as T_2 relaxation, or spin-spin relaxation.

In the T_2 process, nuclei exchange energy with each other and the spins lose phase coherence. Therefore to first order the net magnetization in the xy -plane decays exponentially to zero over time. The rate at which this occurs is dependent on T_2 (Fig. 1B) and the T_2 process is described as:

$$M_{xy}(t) = M_{xy_{\max}} e^{-\frac{t}{T_2}} \quad (1.2)$$

In reality the signal will decay at shorter relaxation time T_2 due to field inhomogeneities and magnetic susceptibility differences. This shorter relaxation time is known as T_2^* , and can be determined according to

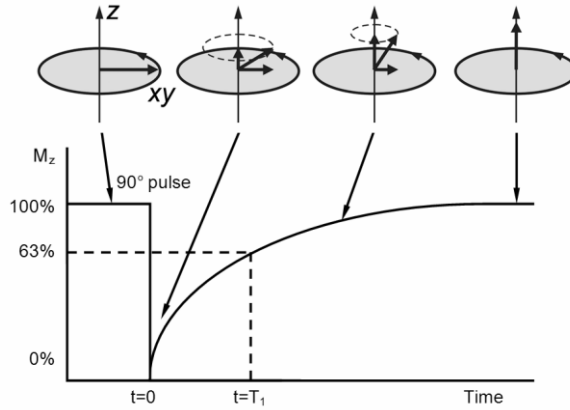
$$\frac{1}{T_2^*} = \frac{1}{T_2} + \frac{1}{T_{2M}} + \frac{1}{T_{2MS}} \quad (1.3)$$

Here T_{2M} is the dephasing due to inhomogeneity of the applied field, and T_{2MS} is the dephasing due to magnetic susceptibility differences (40).

An RF coil placed perpendicular to the transverse plane will detect the transverse component of the net magnetization vector as it precesses around B_0 . The length of the magnetization vector is the magnitude of the signal, while the angle between the magnetization vector and the y-axis is referred to as the the transverse plane after a single RF pulse is known as the free induction decay. Depending on the sample the FID can contain multiple resonance frequencies. A simple spectrum can be obtained from the FID by converting it from the time domain to the frequency domain using the Fourier transform. The resulting spectrum contains peaks for the various different frequencies contained within the FID.

To spatially resolve the NMR signal for MRI, an additional step is required. Spatial variations in frequencies can be translated to spatial information and subsequently to an image. Assigning spatial information to the spins is achieved by adding a magnetic field gradient inside the MR scanner. The gradient field in MRI is usually parallel to B_0 . The gradient has three components, G_x , G_y , and G_z , associated with the x , y , or z spatial axis, respectively. The spins experience different field strengths depending on where they are within the gradient field. Positional dependence of the field strength and resonance frequencies can be calculated according to:

(A)



(B)

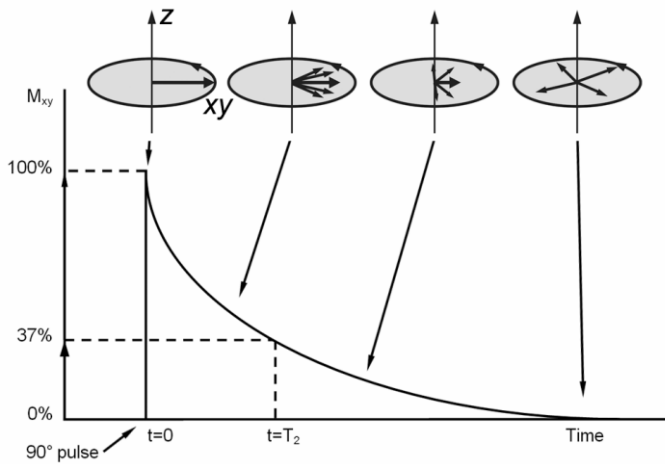


Figure 1.1 (A): Re-growth of the longitudinal magnetization M_z and the definition of T_1 ; M_z will return to its original distribution along the z -axis through T_1 relaxation (eq. 1.1) . (B) Decay of the transverse magnetization M_{xy} and the definition of T_2 ; Loss of phase coherence, and thereby loss of magnetization in the xy -plane, is determined by T_2 relaxation (eq. 1.2).

$$B(\mathbf{r}) = B_0 + rG \quad (1.4)$$

$$\omega(\mathbf{r}) = \gamma B(\mathbf{r}) = \gamma B_0 + \gamma rG \quad (1.5)$$

Here $B(\mathbf{r})$ and $\omega(\mathbf{r})$ are the position dependent field strength and resonance frequency, respectively. The position in the magnetic field is denoted by the vector \mathbf{r} and the magnitude and direction of the gradient is represented by \mathbf{G} (1.4). Spins in different volume units within the field gradient experience a different magnetic field, and are associated with a different Larmor frequency. The selection of the desired cross-section or “slice” is achieved by applying a gradient along the z -axis in combination with an excitation pulse of a convenient bandwidth and shape (*e.g.* Sinc or hermite). This RF pulse excites only the spins in the desired slice, while leaving adjacent spins unaffected, as they have a different resonance frequency due to the applied z -gradient. Within the acquired slice, x - and y -gradients are applied to assign the spins at each position within the slice with a unique frequency and phase. The gradients in this example are often referred to as the slice selection- (G_z), the frequency encoding- (G_x) and the phase encoding gradients (G_y). G_x is usually kept constant over the course of an experiment, thus assigning a different frequency to each position along the x -axis. G_y is stepped a number of times each scan, depending on the desired resolution in the y -direction. G_y applies a specific phase angle to the transverse magnetization vector. While G_y is switched on, each transverse magnetization vector has its own unique Larmor frequency. When G_y is subsequently switched off, the spins return to the frequency they had prior to phase encoding, however, the phase angle of each transverse magnetization vector is different. A variety of imaging pulse sequences can

be created by combining slice selection, phase encoding and frequency encoding.

What distinguishes the T_2 process from its T_1 counterpart is that the magnitude of the field changes over the dephasing period is important, rather than the rate of their fluctuations. As far as biological tissue imaging is concerned, nature offers us a convenient handle in the form of T_1 and T_2 for constant discrimination. Generally, T_2 values are about one-tenth of the T_1 values for soft biological tissues, which have sufficiently different T_2 values to allow them to be differentiated by contrast on T_2 -weighted images.

Among the most important and widely used pulse sequences for MRI are the spin echo sequence and the gradient echo sequence. Gradient Echo (GE) sequences use slice selective pulses of 90° or less, and subsequently employ the gradient coils for producing an echo (Fig. 1.2). This is done by first applying a negative frequency-encoding gradient, which is subsequently reversed, causing the spins to rephase and form an echo. Following signal detection the phase coherence of the precessing spins in the transverse plane is dephased or “spoiled” using spoiler gradients, thus ensuring contribution of only the longitudinal magnetization to the net magnetization \mathbf{M} at the time of the next excitation pulse (40). Conversely, SE sequences use a slice selective 90° pulse for excitation, followed by a 180° pulse at $t = TE/2$. The 180° pulse serves to reverse or refocus the transverse magnetization. This produces an echo at $t = TE$. During SE acquisition, the phase encoding gradient is applied following the 90° pulse, and the frequency encoding, or read out-, gradient is applied centered around the echo at $t = TE$ (40). The TE in these examples is the echo time, and is measured from the center of the excitation pulse to the center of the echo. As multiple excitation-refocus-

echo steps are needed to build up an entire image, the sequence is looped several times, depending on the desired resolution. The repetition time is defined as the time from the start of one loop of the sequence to the next.

1.3.1 Rapid acquisition with relaxation-enhancement imaging

Rapid acquisition with relaxation-enhancement imaging (41) is a fast spin echo imaging sequence in which multiple spin echoes are generated by employing multiple 180° refocusing pulses (Fig. 1.2). Each refocused echo is acquired after having experienced a different phase-encoding value.

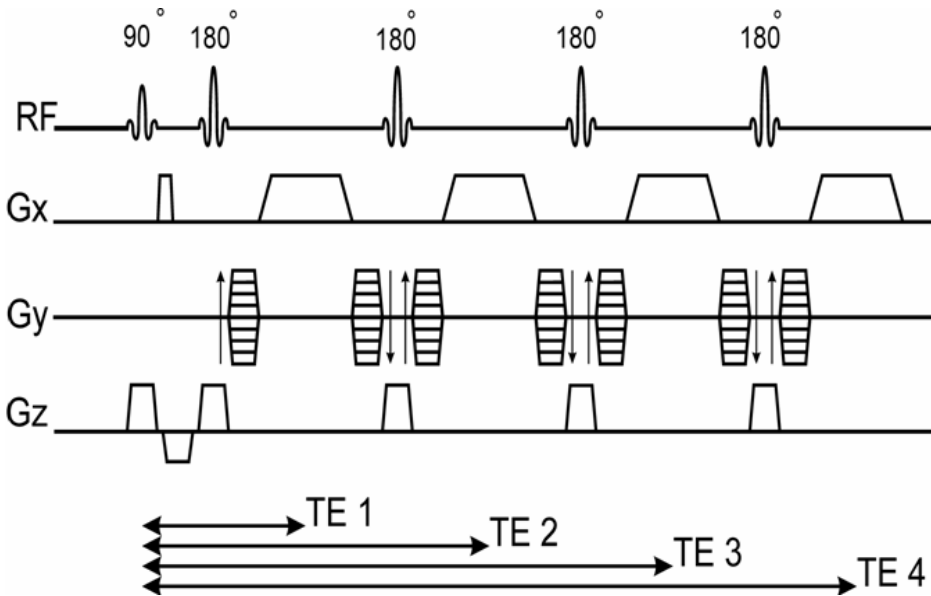


Figure 1.2: RARE pulse sequence: A four-segment (RARE factor of 4) version is shown. Each cycle has four phase encoding steps; the sequence will be looped until the desired number of phase encoding steps is reached. As this sequence acquires four times the data per loop as a standard SE sequence, the scan time is roughly 25% shorter than for an equivalent SE sequence. The effective TE is the TE time during which the $G_y = 0$ lines of data are acquired (4).

Because refocusing of the transverse magnetization is inherent in the sequence, it is less vulnerable to susceptibility-induced dephasing than gradient echo sequences, but it is substantially faster to apply than a spin-echo sequence with a single-phase encoding step per repetition time.

The primary contrast is T_2 -based, although this can be mixed with T_1 and perfusion effects by combining it with the inversion recovery sequence (IR-RARE). The contrast in the final image can be modified depending on the choice of TE and TR. Choosing a long TR, and a relatively long TE, for example, will yield a T_2 -weighted image, where elements with long T_2 will appear bright, and elements with a short T_2 will appear dark. A practical implementation of RARE imaging in visualizing *in vivo* zebrafish is demonstrated in chapter 2 and 4.

1.3.2 Transverse relaxation mapping

Intrinsic MR parameters, such as transverse (T_2) relaxation times are sensitive to changes in the biophysical environment of water, and are thought to be affected during impaired cell physiology. Disease mechanisms influence the composition of tissue, and can have an effect on the tissue specific relaxation rates. Thus T_2 mapping can be used to diagnose or predict disease. For example, T_2 mapping can be used to delineate the disease volume. The regional distribution of T_2 values within a tumor is a measure of the tissue heterogeneity within the tumor volume (42). In addition, the large differences in T_2 relaxation times between normal and diseased tissue can be used in a computer algorithm to automatically demarcate the boundary of abnormal tissue.

Since the polarization present in the xy -plane depends on T_2 , while different T_2 -weighting factors are obtained by modifying the TE value of a spin echo technique, it is possible to calculate the value of T_2 from a series of SE images with different echo times. As the signal intensity in these images is related to the magnetization in the xy plane, T_2 can be calculated by substituting the measured signal intensity for $M_{xy}(t)$, according to

$$M_{xy}(t) = M_{xy_{\max}} e^{-\frac{t}{T_2}} \quad (1.6)$$

where t equals the experimental TE mentioned above.

This can be calculated for the individual voxels of the sample, thus creating a T_2 map, or for specific regions of interest, by averaging the signal intensities for the pixels located within the ROI, and calculating the average T_2 for that region. Since an SE technique is used here, the signal is rephased before detection, which causes the effects of field inhomogeneities and susceptibilities to cancel. Hence, the calculated T_2 is the “true” T_2 and not T_2^* . In chapter 4, T_2 mapping was used to monitor the heterogeneity of the tumors in zebrafish.

1.4 Magnetic Resonance Spectroscopy

In vivo magnetic resonance spectroscopy (MRS) is a unique method providing quantitative biochemical information from the selected volume of interest (VOI) inside the body non-invasively. It provides vital biological information at the molecular level. Combined with magnetic resonance imaging (MRI), an integrated MRI/MRS examination provides anatomical

structure, pathological function, and biochemical information about a living system. MRS provides a link between the biochemical alterations and the pathophysiology of disease. MRS has been widely applied in human and animal studies examining a variety of tissues (43-47).

The fundamental basis of MRS is governed by the same principles of nuclear magnetic resonance (NMR) (48, 49). MRS requires a magnetic field and a radio frequency (RF) transmit pulse at a particular resonant frequency to observe the signal of a specific nucleus (*e.g.*, ^1H , ^{31}P , ^{13}C etc.) in the region of interest. The product of MRS is a “spectrum” with a frequency axis in parts per million (ppm) and a signal amplitude axis (50-54). The signal amplitude measures a particular metabolite concentration. Specific nuclei (*e.g.*, ^1H) from the metabolite, depending on their characteristic signature, give rise to either a single peak or multiple peaks that are uniquely shifted along the frequency axis, depending on their chemical environment. The shift dispersion increases with magnetic field strength. *In vivo* ^1H MRS and ^{31}P -MRS are the most widely used applications of MRS, but other nuclei that are used for MRS studies include ^{13}C , ^{15}N , ^{19}F , and ^{23}Na .

A wide variety of spatial localization techniques are in use to localize the spectroscopic measurement in a specific volume of interest, or voxel. These methods rely on the spatial selection of slices by the application of frequency-selective RF pulses in the presence of a magnetic field gradient. Some of them require several acquisitions to achieve complete localization, whereas others can achieve localization in a single experiment (39). Among the most popular methods is point resolved spectroscopy (55, 56). The PRESS sequence is a double spin-echo sequence. Three slice-selective

pulses (90° , 180° , 180°) along three orthogonal axes define three orthogonal slices, and make it possible to localize the signal in the voxel formed by the intersection of the three slices. Outer volume suppression schemes excite narrow slices positioned around the volume of interest to selectively remove unwanted signals from outside the voxel. Following slice selective excitation, the transverse magnetization in these slices is dephased by a subsequent magnetic field crusher gradient. OVS is most commonly employed to remove lipid signals from the spectrum (39). As water is the most abundant compound in tissue, the NMR proton spectrum of almost all tissue is dominated by a resonance at ~ 4.7 ppm that originates from water protons. While metabolite detection is possible without water suppression, the water peak does lead to baseline distortions and spurious signals due to vibration-induced signal modulation, which makes the detection of metabolites unreliable (39). Suppression of the water signal eliminates these problems, leading to a reliable and consistent detection of metabolite spectra. Water signals can be eliminated by utilizing differences in relaxation parameters. One such method, VAPOR, combines T_1 -based water suppression and optimized frequency-selective perturbations to provide excellent water suppression with a large insensitivity towards T_1 and B_1 inhomogeneity (39, 57). The combination of OVS and water suppression improves localization performance and reduces the demand for spoiler gradients (57). The PRESS sequence in combination with water and outer volume suppression schemes has been optimized for zebrafish brain in chapter 3.

MRS techniques have been developed and applied extensively in brain research (58). The brain has multiple levels of compartmentation ranging from the type of cellular compartment (neuron versus astrocyte) to the type

of tissue compartment (the gray matter vs. the white matter). These compartments are highly integrated and work together to attain various brain functions. MRS is useful in understanding the neurochemical changes in the brain due to different physiological processes. Many MRS applications have been reported exclusively in the brain due to the lack of motion artifacts in the brain. In addition, the brain is more or less spherical; hence, it is easier to adjust to a high degree of homogeneity of the magnetic field by shimming for MRS studies. However, there are susceptibility differences in the brain between the intracellular and extracellular space. The problems with sensitivity and susceptibility differences can become more serious when considering small zebrafish brain.

1.5 MRI/MRS at ultra-high magnetic field

Magnetic field strengths for *in vivo* MRI and MRS have seen a steady increase, and are currently up to 9.4 T for humans and 17.6 T for animals. This drive has largely been fueled by the greatly improved contrast-to-noise (CNR) ratio of functional MRI (fMRI) techniques, as well as the linear increase in signal-to-noise (SNR) ratio and spectral resolution with increasing field strength (59).

Since T_1 and T_2 relaxation parameters play an important role in the actual SNR and resolution, they should be critically considered while imaging at high-magnetic field. In general, T_1 relaxation times increase with increasing field strength, while the absolute differences between tissue T_1 's become somewhat smaller. Therefore, overall the T_1 contrast will decrease at higher magnetic fields. However, since the SNR is improved at higher magnetic fields, the CNR is typically higher. It has been demonstrated in earlier

studies that even at 9.4 T and 11.7 T high-quality T_1 -weighted images can be obtained from rat brain (59), in close analogy to high-quality T_1 -weighted human brain images reported at 7 T (60). Thus T_1 -weighting remains a valuable image contrast mechanism even at very high magnetic fields. Water T_2 relaxation times decrease dramatically in high magnetic field. The relative differences in tissue T_2 's remain the same or actually increase with increasing field strength. Therefore, while it may be more difficult to attain the shorter TE's required, T_2 weighting is a viable high-field image contrast mechanism, as shown by the excellent T_2 contrast obtained at 9.4 T in previous studies (61). For NMR spectroscopy a higher magnetic field strength is always desirable. The spectral resolution and the quantification accuracy of metabolites, especially those with strongly coupled spins and those present in low concentration, will continue to improve in moving toward increasingly high magnetic fields. Therefore, both the information content and the quantification accuracy of metabolites will improve at higher magnetic fields.

Thus, the use of high magnetic fields will be highly beneficial for MR imaging as well as MR spectroscopy of zebrafish. This can be achieved by using high (9.4T) and ultra-high magnetic fields (17.6T) in combination with strong magnetic field gradients and the use of small, high-sensitivity RF coils to achieve the necessary sensitivity.

1.6 Scope of the thesis

The necessity to study an adult zebrafish non-invasively and the recent developments in the field of MR microimaging and spectroscopy has brought us to use MR microimaging and spectroscopy as analysis tools to

visualize anatomical and molecular details of live adult zebrafish. Although a large pool of genome wide studies in zebrafish at early embryonic stages is available, *in vivo* studies in adult zebrafish are missing. Non-invasive studies of adult zebrafish performed in this thesis provide a means to bridge the gap between genetic studies at early embryonic stages and the structural and functional investigations at the adult stages. The specific aim of this thesis is to implement and optimize high resolution MR microimaging methods to obtain *in vivo* anatomical information from adult zebrafish. These methods were then successfully applied to investigate the presence of internal tumors in transgenic zebrafish. In addition, *in vivo* MR spectroscopy has been applied to detect metabolites in adult zebrafish brain for the first time.

In **chapter 2**, high-field μ MRI methods have been optimized and successfully implemented to visualize anatomical details of adult zebrafish *in vivo*. Described in **chapter 3** is the implementation and optimization of a localized 1D MR spectroscopic sequence, at 9.4T. Using this sequence, highly resolved 1D MR spectra were obtained, for the first time, from the adult zebrafish brain *in vivo*. In **chapter 4**, μ MRI was applied to track spontaneous melanomas in stable transgenic zebrafish model expressing a RAS oncoprotein and lacking P53. The heterogeneity of the tumor has been probed by measuring T_2 relaxation times in different regions of the tumors. **Chapter 5** provides a general discussion to the work presented in this thesis, and presents some future prospects.

References

1. Nolan PM, Peters J, Strivens M, Rogers D, Hagan J, Spurr N, Gray NC, Vizor L, Brooker D, Whitehill E, Washbourne R, Hough T, Greenaway S, Hewitt M, Liu X, McCormack S, Pickford K, Selley R, Wells R, Tymowska-Lalanne Z, Roby P, Glenister P, Thornton C, Thaug C, Stevenson JA, Arkell R, Mburu P, Hardisty R, Kiernan A, Erven A, Steel KP, Voegeling S, Guenet JL, Nickols C, Sadri S, Naase M, Isaacs A, Davies K, Browne M, Fisher EMC, Martin J, Rastan S, Brown SDM, Hunter J. A systematic, genome-wide, phenotype-driven mutagenesis programme for gene function studies in the mouse. *Nature Genet* 2000; 25:440–443.
2. Hrabe de Angelis MH, Flaswinkel H, Fuchs H, Rathkolb B, Soewarto D, Marschall S, Heffner S, Pargent W, Wuensch K, Jung M, Reis A, Richter T, Alessandrini F, Jakob T, Fuchs E, Kolb H, Kremmer E, Schaeble K, Rollinski B, Roscher A, Peters C, Meitinger T, Strom T, Steckler T, Holsboer F, Klopstock T, Gekeler F, Schindewolf C, Jung T, Avraham K, Behrendt H, Ring J, Zimmer A, Schughart K, Pfeiffer K, Wolf E, Balling R. Genome-wide, large-scale production of mutant mice by ENU mutagenesis. *Nature Genet* 2000; 25:444–447.
3. Michaud EJ, Culiati CT, Klebig ML, Barker PE, Cain KT, Carpenter DJ, Easter LL, Foster CM, Gardner A, Guo ZY, Houser KJ, Hughes LA, Kerley MK, Liu Z, Olszewski RE, Pinn I, Shaw GD, Shinpock SG, Whyemore A, EM Rinchilk, Johnson DK. Efficient gene-driven germ-line point mutagenesis of C57BL/6J mice. *BMC Genomics* 2005; 6:164.
4. Carpinelli MR, Hilton DJ, Metcalf D, Antonchuk JL, Hyland CD, Mifsud SL, Rago LD, Hilton AA, Willson TA, Roberts AW, Ramsay RG, Nicola NA, Alexander WS. Suppressor screen in *Mpl*^{-/-} mice: *c-Myb* mutation causes supraphysiological production of platelets in the absence of thrombopoietin signaling. *Proc Natl Acad Sci USA* 2004; 101:6553–6558.

5. Coghill EL, Higill A, Parkinson N, Davison C, Glenister P, Clements S, Hunter J, Cox RD, Brown SDM. A gene-driven approach to the identification of ENU mutants in the mouse. *Nature Genet* 2002; 30:255–256.
6. Quwailid MM, Hugill A, Dear N, Vizor L, Wells S, Horner E, Fuller Shelly, Weedon J, McMath H, Woodman P, Edwards D, Campbell D, Rodger S, Carey J, Roberts A, Glenister P, Lalanne Z, Parkinson N, Coghill EL, Mckeone R, Cox S, Willan J, Greenfield A, Keays D, Brady S, Spurr N, Gray I, Hunter J, Brown SDM, Cox RD. A gene-driven ENU based approach to generating an allelic series in any gene. *Mamm Genome* 2004; 15: 585–591.
7. Van der Sar AM, Appelmelk BJ, Vandenbroucke-Grauls CM, Bitter W. A star with stripes: zebrafish as an infection model. *Trends Microbiol* 2004;12:451–457.
8. Langenau DM, Zon LI. The zebrafish: a new model of t-cell and thymic development. *Nat Rev Immunol* 2005;5:307–317.
9. Westerfield M. *The Zebrafish book. A guide for the laboratory use of Zebrafish (Danio rerio)*. University of Oregon Press:Eugene, OR, 1995.
10. Zon LI, Peterson RT. *In vivo* drug discovery in the zebrafish. *Nat.Rev. Drug Discov.* 2005; 4(1): 35–44.
11. Goldsmith P. Zebrafish as a pharmacological tool: the how, why and when. *Current Opinion in Pharmacology* 2004; 4(5): 504–512.
12. Ankley GT, Johnson RD. Small fish models for identifying and assessing the effects of endocrine-disrupting chemicals. *ILAR J.* 2004; 45(4): 469–483.
13. Kent ML, Spitsbergen JM, Matthews JM, Fournie JW, Westerfield M. Diseases of zebrafish in research facilities. *Zebrafish International Resource Center* 2002. Available from: <http://zebrafish.org/zirc/health/diseaseManual.php>.
14. Amatruda JF, Shepard JL, Stern HM, Zon LI. Zebrafish as a cancer model system. *Cancer Cell* 2002; 1:229-231.

15. Langenau DM, Keefe MD, Storer NY, Guyon JR, Kutok JL, Le X, Goessling W, Neuberg DS, Kunkel LM, Zon LI. Effects of RAS on the genesis of embryonal rhabdomyosarcoma. *Genes Dev* 2007;21:1382 – 1395.
16. Smolowitz R, Hanley J, Richmond H. A three-year retrospective study of abdominal tumors in zebrafish maintained in an aquatic laboratory animal facility. *Biol Bull* 2002;203:265 –266.
17. Stern HM, Zon LI. Cancer genetics and drug discovery in the zebrafish. *Nature Reviews Cancer* 2003;3:1-7.
18. Berghmans S, Murphey RD, Wienholds E, Neuberg D, Kutok JL, Fletcher CDM, Morris JP, Liu TX, Schulte-Merker S, Kanki JP, Plasterk R, Zon LI, Look AT. tp53 mutant zebrafish develop malignant peripheral nerve sheath tumors. *Proc Natl Acad Sci U S A* 2005;102:407 – 412.
19. Goessling W, North TE, Zon LI. Ultrasound biomicroscopy permits *in vivo* characterization of zebrafish liver tumors. *Nat Methods* 2007; 4:551-553.
20. Kari G, Rodeck U, Dicker AP. Zebrafish: an emerging model system for human disease and drug discovery. *Clin Pharmacol Ther* 2007; 82: 70–80.
21. Haldi M, Ton C, Seng WL, McGrath P. Human melanoma cells transplanted into zebrafish proliferate, migrate, produce melanin, form masses and stimulate angiogenesis in zebrafish. *Angiogenesis* . 2005; 9: 139–151.
22. Lee LM, Seftor EA, Bonde G, Cornell RA, Hendrix MJ. The fate of human malignant melanoma cells transplanted into zebrafish embryos: assessment of migration and cell division in the absence of tumor formation. *Dev Dyn* 2005; 233: 1560–1570.
23. Topczewska JM, Postovit LM, Margaryan NV, Sam A, Hess AR, Wheaton WW, Nickoloff BJ, Topczewski J, Hendrix MJC. Embryonic and tumorigenic pathways converge via Nodal signaling: role in melanoma aggressiveness. *Nat Med* 2006;12: 925–932.
24. Nicoli S, Ribatti D, Cotelli F, Presta M. Mammalian tumor xenografts induce neovascularization in zebrafish embryos. *Cancer Res* 2007; 67: 2927–2931.

25. Stoletov K, Montel V, Lester RD, Gonias SL, Klemke R. High-resolution imaging of the dynamic tumor cell vascular interface in transparent zebrafish. *Proc Natl Acad Sci USA* 2007;104:17406–17411.
26. Parng C, Seng WL, Semino C, McGrath P. Zebrafish: a preclinical model for drug screening. *Assay Drug Dev Technol* 2002;1: 41–48.
27. Ceol CJ, Houvras Y, White RM, Zon LI. Melanoma biology and the promise of zebrafish. *Zebrafish* 2008; 4:247-255.
28. Chin L, Garraway LA, Fisher DE. Malignant melanoma: genetics and therapeutics in the genomic era. *Genes Dev* 2006; 20:2149–2182.
29. Lorigan P, Eisen T, Hauschild A. Systemic therapy for metastatic malignant melanoma—from deeply disappointing to bright future? *Exp Dermatol* 2008;17:383–394.
30. Bretaud S, Allen C, Ingham PW, Bandmann O. p53-dependent neuronal cell death in a DJ-1-deficit zebrafish model of Parkinson’s disease. *J Neurochem* 2007; 100:1626–1635.
31. Tomasiewicz HG, Flaherty DB, Soria JP, Wood JG. Transgenic zebrafish model of neurodegeneration. *J Neurosci Res* 2002;70:734-745.
32. Panula P, Sallinen V, Sundvik M. Modulatory neurotransmitter systems and behavior: towards zebrafish models of neurodegenerative diseases. *Zebrafish* 2006;3:235-247.
33. Campbell WA, Yang H, Zetterberg H. Zebrafish lacking Alzheimer presenilin enhancer 2 (Pen-2) demonstrate excessive p53-dependent apoptosis and neuronal loss. *J Neurochem* 2006; 96:1423-1440.
34. Bai Q, Mullett SJ, Garver JA, Hinkle DA, Burton EA. Zebrafish DJ-1 is evolutionarily conserved and expressed in dopaminergic neurons. *Brain Res* 2006; 1113:33-44.
35. Rupp B, Wullimann MF, Reichert H. The zebrafish brain: a neuroanatomical comparison with the goldfish. *Anat Embryol* 1996;194: 187–203.

36. Flinn L, Bretaud S, LO C, Ingham PW, Bandmann O. Zebrafish as a new animal model for movement disorders. *Journal of Neurochemistry* 2008; 106: 1991-1997.
37. Levitt MH. *Spin dynamics: basics of nuclear magnetic resonance*, 1st ed. Wiley 2001, Chichester, UK.
38. Haacke EM, Brown RW, Thompson MR, Venkatesan R. *Magnetic resonance imaging: physical principles and sequence design*, 1st ed. Wiley-Liss 1999, Hoboken, USA.
39. De Graaf RA. *In vivo NMR spectroscopy: principles and techniques*, 2nd ed. Wiley 2008; Chichester, UK.
40. Brown MA, Semelka RC. *MRI: basic principles and applications*, 3rd ed. Wiley-Liss 2003, Hoboken, USA.
41. Hennig J, Nauerth A, Friedburg H. Rare imaging - a fast imaging method for clinical MR. *Magn Reson Med* 1986;3:823-833.
42. Bloch P, Lenkinski RE, Buhle, Jr. EL, Hendrix R, Bryer M, McKenna WG. The use of T_2 distribution to study tumor extent and heterogeneity in head and neck cancer. *Magn Reson Imaging* 1991; 9:205-211.
43. Boesch C. Musculoskeletal spectroscopy. *J Magn Reson Imaging* 2007;25(2):321-338.
44. Cecil KM. MR spectroscopy of metabolic disorders. *Neuroimaging clinics of North America* 2006;16(1):87-116.
45. Choi JK, Dedeoglu A, Jenkins BG. Application of MRS to mouse models of neurodegenerative illness. *NMR in biomedicine* 2007; 20(3):216-237.
46. Rosen Y, Lenkinski RE. Recent advances in magnetic resonance neurospectroscopy. *Neurotherapeutics* 2007;4(3):330-345.
47. Sibtain NA, Howe FA, Saunders DE. The clinical value of proton magnetic resonance spectroscopy in adult brain tumours. *Clinical radiology* 2007;62(2):109-119.
48. Ernst R. Nuclear magnetic double resonance with an incoherent radio-frequency field. *J Chem Phys* 1966; 45:3845-3861.

49. Mandal PK, Majumdar A. A comprehensive discussion of HSQC and HMQC pulse sequences. *Concepts Magn Reson* 2004; Part A 20A:1–23.
50. Pettegrew JW, Panchalingam K, Moossy J, Martinez J, Rao G. Correlation of phosphorus-31 magnetic resonance spectroscopy and morphologic findings in alzheimer's disease. *Arch Neurol* 1988; 45: 1093–1096.
51. Moonen CT, von Kienlin M, van Zijl PC, Cohen J, Gillen J. Comparison of single-shot localization methods (STEAM and PRESS) for *in vivo* proton NMR spectroscopy. *NMR Biomed* 1989; 2:201–208.
52. Van der Toorn A, Dijkhuizen RM, Tulleken CA, Nicolay K. T_1 and T_2 relaxation times of the major ^1H -containing metabolites in rat brain after focal ischemia. *NMR Biomed* 1995;8:245–252.
53. Stanley JA. *In vivo* magnetic resonance spectroscopy and its application to neuropsychiatric disorders. *Can J Psychiatry* 2002;47:315–326.
54. Moonen CTW, Sobering G, Vanzijl PCM, Gillen J, Vonkienlin M, Bizzi A. Proton spectroscopic imaging of human brain. *J Magn Reson* 1992; 98:556–575.
55. Bottomley PA. Selective volume method for performing localized NMR spectroscopy. US patent 1984;4:480-228.
56. Bottomley PA. Spatial localization in NMR spectroscopy *in vivo*. *Ann N Y Acad Sci* 1987; 508:333-348.
57. Tkac I, Starcuk Z, Choi IY, Gruetter R. *In vivo* H-1 NMR spectroscopy of rat brain at 1 ms echo time. *Magn Reson Med* 1999;41:649-656.
58. Gillies RJ, Morse DL. *In vivo* magnetic resonance spectroscopy in cancer. *Annu Rev Biomed Eng* 2005; 7:287–326.
59. De Graaf RA, Brown PB, McIntyre S, Nixon TW, Behar KL, Rothman DL. High magnetic field water and metabolite proton T_1 and T_2 relaxation in rat brain *in vivo*. *Magnetic Resonance in Medicine* 2006; 56:386–394.
60. Henry PG, Kim SG, Lieu H, Tkac I, Vaughan T, Van De Moortele PF, Yacoub E, Zhu XH. Ultrahigh field magnetic resonance imaging and spectroscopy. *Magn Reson Imaging* 2003;21:1263–1281.

61. Braakman N, Matysik J, van Duinen SG, Verbeek F, Schliebs R, de Groot HJM, Alia A. Longitudinal assessment of alzheimer's β -Amyloid plaque development in transgenic mice monitored by *in vivo* magnetic resonance microimaging. J Magn Res Imaging 2006;24:530-536.

2 Magnetic Resonance Microimaging of the Adult Zebrafish^{*}

2.1 Abstract

Magnetic resonance microimaging (μ MRI) is an imaging modality that allows acquisition of high-resolution images in intact opaque animals non-invasively. The zebrafish (*Danio rerio*) is an important model organism for the study of vertebrate biology. However, optical *in vivo* studies in zebrafish are restricted to very early developmental stages due to opaqueness of the juvenile and the adult stages. Application of high resolution μ MRI has not yet been explored in adult zebrafish. In this study we applied and optimized high resolution μ MRI methods to examine anatomical structures non-invasively in adult zebrafish. Clear morphological proton images were obtained by T_2 -weighted spin echo and rapid acquisition with relaxation enhancement (RARE) sequences revealing many anatomical details in the entire intact zebrafish at 9.4T. In addition, *in vivo* imaging of adult zebrafish revealed sufficient anatomical details. To our knowledge this is the first report for the application of high resolution μ MRI to study detail anatomical structures in adult zebrafish.

**This chapter was published in Zebrafish 2006; 3:431-439*

2.2 Introduction

The zebrafish has emerged as an excellent model organism for studies of vertebrate evolution, diseases, biological pathways, and toxicological mechanisms (1, 2). The near completion of the zebrafish genome sequence and the EST sequencing project allow the use of the versatile morpholino-based antisense knock-down approach to rapidly analyse the function of many different gene products within the first five days of zebrafish development. External development and optical clarity during embryogenesis allow for visual analysis of early developmental processes, and high fecundity and short generation times facilitate genetic analysis. However, due to opaqueness of juvenile and adult stages, traditional optical microscopic methods are not suitable to study various developmental processes in adult zebrafish. Alternative methods of analysis are invasive; fish are sacrificed and processed to reveal specific information like morphology, histology, gene expression pattern and physiological parameters during normal and abnormal conditions such as stress and infection. In addition, development and progression can not be studied over time in the same fish and analysis has to be repeated on different individuals. At present, no high resolution images of the complete juvenile and adult histology of the zebrafish are available, neither in internet accessible databases nor in the literature. Unavailability of such resources is amongst other things due to difficulties in the imaging of larger areas of interest and an extra complication is experienced in deformation of the specimen in the preparation process causing distortion, artefacts and degradation of spatial resolution (3-5). These raise a need for a rapid sensitive and non-invasive imaging methods to follow developmental or other processes, not only of the embryonic phase but also of juvenile and adult stages and to establish an anatomical atlas of adult zebrafish.

Magnetic resonance microimaging (μMRI) is an imaging technique that explores the nuclear magnetic characteristics of the abundant protons in tissue (6). It is a non-invasive, non-ionizing imaging modality that has unique three-dimensional capabilities and allows acquisition of high-resolution images non-invasively in intact opaque animals (7-10). μMRI is founded on the same fundamental principles as MRI but produces images with higher spatial resolution because of the use of strong magnetic field gradients (200-1000 mT/m) and specialized radio frequency (RF) coils (11-13). For example, a spatial resolution of 20 μm³ per voxel can be achieved. μMRI offers the possibility to image a live adult fish non-invasively, which is impossible using other imaging techniques. With μMRI, it is possible to study developmental processes over an extended period of time in the same fish from embryo till adulthood. μMRI can also be very attractive and suitable for functional imaging investigations in zebrafish. With the help of μMRI it is also possible to image the blood flow and to do local molecular spectroscopy like measurement of ATP and ADP concentration (6, 14). *In vivo* visualization of gene expression by MRI in combination of contrast agents in a living embryo of *X. laevis* has been demonstrated earlier (5).

High resolution μMRI has not yet been exploited for imaging adult zebrafish. The objective of the present study is to optimize the MR setup and μMRI sequences to visualize high resolution structural details in adult zebrafish *in vitro* which can be extended later to an *in vivo* system. Because of the very small size compared to a mouse or a rat, imaging of adult zebrafish needs high resolution. To achieve this, we used a high field of 9.4T for μMRI study of adult zebrafish. In addition to *ex vivo* studies, a flow-through setup has been designed for *in vivo* μMRI studies of adult

zebrafish and first results of *in vivo* μ MRI are presented. We demonstrate that high field μ MRI provides sufficient resolution to get rapid access to anatomical details in adult zebrafish in a short time. This paves the way for studying disease development, biological pathways, and toxicological mechanisms during various developmental stages in individual living zebrafish.

2.3 Materials and methods

Zebrafish

Adult Wild-type zebrafish (*Danio rerio*) were maintained in recirculating aquarium systems according to established rearing procedures (15, 16). The water temperature was maintained at 28 °C with a flow rate of 150 L/min, with day/night light cycles (12h dark versus 12h light). The fish were fed twice daily with commercial flake food according to Westerfield (2000) (16). All fish were handled according to Institutional Animal Care and Use Committee guidelines. For *ex-vivo* imaging, adult zebrafish were euthanized and immediately embedded in Fomblin (Perfluoropolyether). Alternatively, the fish were fixed in 4% buffered paraformaldehyde (Zinc Formal-Fixx, ThermoShandon, UK) for 2 days and subsequently embedded in Fomblin.

Experimental setup for in vivo imaging

For *in vivo* MRI measurements, fish was anesthetised by adding 0.01% MS222 (ethyl meta aminobenzoate metanesulfonic acid salt; Sigma chemical co.) to pH controlled water. Subsequently fish was transferred to a closed flow-through chamber, which was designed for continuous flow of aerated water to support living zebrafish inside the magnet. The flow-

through setup was then inserted in the centre of the volume coil (2 cm diameter) inside the microimaging probe, which was then inserted in the bore of the vertical MR magnet (400 MHz). Aerated water with anaesthetic was pumped from a temperature controlled aquarium to a tube fixed on lower end of the flow-through cell, which was close to the mouth of the fish. After passing the chamber the water was transported back to the aquarium. The setup allowed direct *in vivo* NMR measurements at constant flow speeds (20 ml/min) which were regulated by a STEPDOS 03/08 pump (KNF Flodos AG, Switzerland). After the MRI measurements, zebrafish were transferred back to normal aquarium without anaesthetic where fish recovered uneventfully from the experimental treatment.

Magnetic resonance microimaging

MR imaging was performed using a 400 MHz (9.4T) vertical bore system, using a 20 mm volume coil and a 1 Tm^{-1} gradient insert from Bruker Analytic, Germany. Before each measurement the magnetic field homogeneity was optimized by shimming. Each session of measurements began with a multislice orthogonal gradient-echo sequence for position determination and selection of the desired region for subsequent experiments.

Various MRI scan protocols were used and optimized for high resolution imaging of zebrafish. T_2 -weighted multi slice multi echo (MSME) and Rapid Acquisition with Relaxation Enhancement (RARE) (17) sequences were used for the *ex vivo* imaging of adult zebrafish. For *in vivo* imaging, the RARE sequence was used. The FOV was varied from 1 cm to 3.5 cm with an image matrix of 256×256 . Data acquisition and processing were performed with Para Vision 3.02pl (Bruker Biospin, Germany) running on a

Silicon Graphics 02 workstation with the Irix 6.5.3 operating system and using a Linux pc running XWinNMR 3.2.

3D reconstruction

A 3D image of adult zebrafish has been reconstructed from a series of 2D MR slices with the help of 3D reconstruction software, TDR-3D base (18). The images are imported in the TDR-3D base software as separate 2D images while keeping the coherence of the stack. Using the TDR-3D base software allows to build a contour model using by delineating the structures of interest either manually by digitizer tablet or through automated procedure. The contours are stored in a geometrical database from which other geometrical representations can be generated. MR image files of adult zebrafish containing 25 slices of 0.2 mm thickness with calibrated scale markers were imported in TDR-3D base software. A selection of anatomical domains, *i.e.*, brain, heart, liver and swim bladder, etc. was delineated in the images. The contours in the stack make up the 3D geometrical model that is reconstructed and visualized as a 3D rendering.

2.4 Results

In proton μ MRI, the signal intensity arising from any element (voxel) in the three-dimensional image is typically a function of the water concentration and relaxation time (T_1 , spinlattice relaxation time; T_2 , spin-spin relaxation time) (19). Local variations in these parameters provide the vivid contrast seen in the images obtained by μ MRI, and various anatomical details can be clearly seen.

2.4.1 *Ex vivo* studies

Sagittal slice images of a fixed adult zebrafish were obtained by multislice multiecho (MSME) pulse sequences at 9.4 T using a repetition time of 2000 ms and an echo time of 15 ms. With an anisotropic field of view (FOV) of 20 mm X 35 mm, we obtained a spatial resolution of 137 μ m. Structures including the brain, intestine, swim bladder, and myoseptum can be clearly recognized (Fig. 2.1A). The total scan time used for this set of experiments was 27 minutes. Although this scan time is adequate for high-resolution *ex vivo* imaging, it is not reasonable for imaging living adult zebrafish, which requires very short scan times to ensure the survival of the zebrafish during and after μ MRI measurements.

To reduce the total acquisition time, we explored rapid acquisition using the rapid acquisition with relaxation enhancement (RARE) sequence. RARE is a multiecho imaging sequence in which each refocused echo is acquired after having experienced a different phase-encoding value. This reduces the total imaging time. Because B_0 refocusing is inherent in the sequence, it is less vulnerable to susceptibility-induced dephasing than, for example, gradient echo sequences. In addition, it is substantially faster to apply than a spin-echo sequence with a singlephase encoding value per repetition time (TR). The primary contrast is T_2 -based. Sagittal images of adult zebrafish were obtained with the RARE sequence (Fig. 2.1B). With a RARE factor (echo train length) of 4, a repetition time of 2000 ms, and an echo time of 15 ms (effective, 33.7 ms), we obtained high resolution images in a period as short as 8 minutes, with 4 number of averages resulting in a clear image of head and abdominal structures. Because of very high signal- to-noise ratios in these images, the scan time can be further reduced by taking a smaller

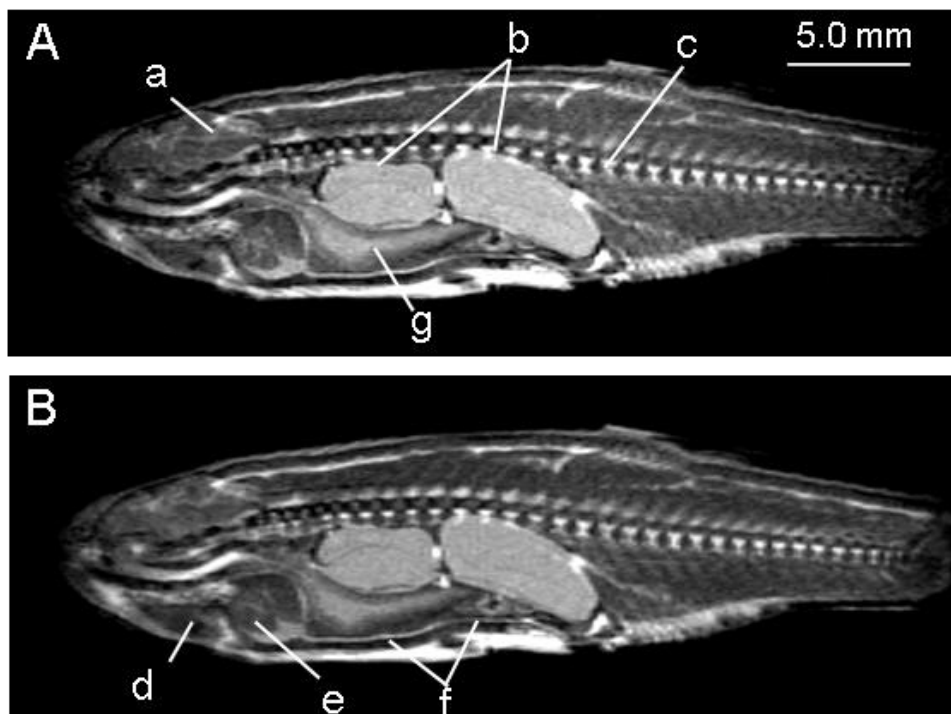


Figure 2.1 High resolution images of adult zebrafish at 9.4T. Slices in the sagittal plane were obtained using the MSME pulse sequence ($TE=15$ ms; $TR=2000$ ms; $ns=4$; T. Scantime 27 min) (A) or RARE sequence ($TE=15$ ms with effective TE 33.6 ms; $TR=2000$ ms; $ns=4$, T. Scantime 8 min) (B). The image resolution is $137\ \mu\text{m}$. Slice thickness 0.2 mm. (a) brain; (b) swim bladder; (c) horizontal myoseptum; (d) heart; (e) stomach; (f) intestine; (g) ovary

number of averages for imaging living zebrafish. Four successive slices of adult zebrafish were obtained in the sagittal (Fig. 2.2A), coronal (Fig. 2.2B), and axial planes (Fig. 2.2C) using the RARE sequence with an image resolution of $78\ \mu\text{m}$. Many anatomical details are clearly visible. The shape of the brain is nicely visible in all three planes. Figures 2.1 and 2.2 were obtained using formalin-fixed adult zebrafish. The formalin fixation process alters tissue characteristics by forming crosslinks between proteins or

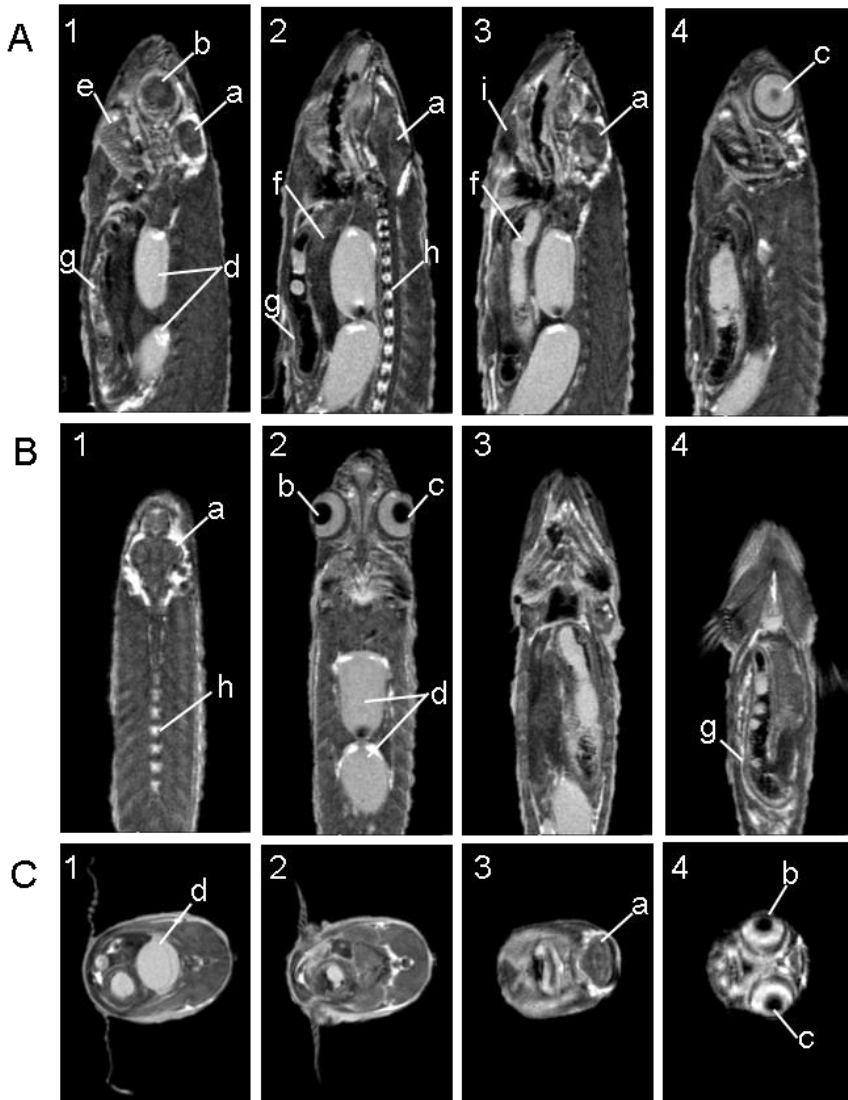


Figure 2.2 High resolution images of adult zebrafish at 9.4T. Successive Slices (1-4) in sagittal (A), coronal (B) and axial (C) planes were obtained using the RARE pulse sequence ($TE= 15$ ms with effective TE 33.6 ms; $TR= 2000$ ms; $ns=4$; T_s Scantime 8 min). The image resolution is $78 \mu\text{m}$. Slice thickness 0.2 mm. (a) brain; (b) left eye; (c) right eye; (d) swim bladder; (e) gills; (f) ovary; (g) intestine; (h) horizontal myoseptum; (i) heart.



Figure 2.3 High resolution images through the head of a fresh unfixed adult zebrafish obtained by a RARE pulse sequence at 9.4T. Successive slices (A-D) in sagittal plane. The image resolution is 78 μm . Slice thickness 0.2 mm (a) eye; (b) brain; (c) horizontal myoseptum; (d) swim bladder; (e) heart; (f) stomach; (g) intestine; (h) eggs.

protein and nucleic acids, and by creating hydroxymethylene bridges and binding of calcium ions (20). For MR imaging, the fixation process enhances contrast. However, to open the possibility of *in vivo* imaging of zebrafish, MR methods were also optimized and applied to zebrafish without fixation. Figure 2.3 shows four slices through the sagittal planes of adult zebrafish taken immediately after death without formalin fixation. Clear differences can be recognized in fixed (Fig. 2.1) and unfixed (Fig. 2.3) zebrafish. For instance, the swim bladder appears black in fresh unfixed zebrafish while in fixed zebrafish they appear white due to penetration of formalin in the swim bladder. Eggs in the ovary are more clearly seen in fresh unfixed zebrafish. Although the overall contrast in MR images of

unfixed zebrafish was less than for fixed zebrafish, it is sufficient to obtain morphological and anatomical details. Figure 2.3 was obtained using the same parameters as the images of the fixed fish, with an image resolution of 78 μm .

2.4.2 *In vivo* studies

On the basis of these optimized protocols for *ex vivo* imaging of zebrafish, we extended our studies to image living adult zebrafish using μ MRI. Although *in vivo* MRI has become an approved tool in medicine and pharmacologic research, very few studies have used this method to uncover physiology in aquatic organisms (21). Aquatic animals require special setups and several precautions for supporting *in vivo* imaging.

For example, fish need a continuous flow of aerated water to irrigate their gills during the MRI measurements. This requires a special watertight flow-through chamber to support the fish and to prevent any contact of water with the RF coil and gradient insert. The fish needs to be immobilized to prevent motion artifacts, either by restraining or using anesthetic. In addition, imaging artifacts due to the surrounding water flow should be minimized. *In vivo* MRI studies in a few aquatic animals such as teleosts (*e.g.*, carp), eelpout, and *Gadus morhua* have been successfully demonstrated (21-24). Due to the small size of zebrafish, additional precautions are needed for *in vivo* imaging. For example, a high-resolution microimaging magnet, needed to get good resolution with small fish, has limited space for a flow-through chamber. The small flow-through chamber cannot support a high flow of water that would be needed if unwanted signal from surrounding water is to be avoided. It has been shown that unwanted signal from surrounded water

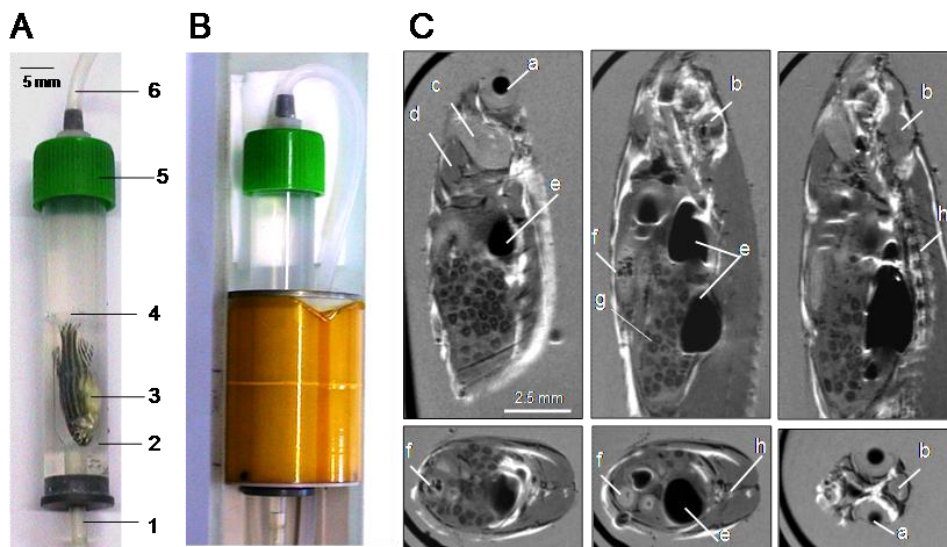


Figure 2.4 (A) Design of flow-through chamber for *in vivo* MRI measurements of living adult zebrafish. 1, water inlet; 2, U-shaped PVC chamber to hold the fish into which water inlet enters from the bottom near the mouth of the fish; 3, a specimen of adult zebrafish; 4, a variable slide barrier to fit the size of the fish with a hole at the bottom; 5, chamber closet; 6, water outlet. (B) Flow-through chamber fitted into the volume coil of microimaging probe. (C) MRI images of anaesthetized living adult zebrafish obtained at 9.4T. Slices in sagittal (upper row) and coronal (lower row) planes were obtained using the RARE pulse sequence (echo train length = 4; TE= 10.5 ms with effective TE 22.5 ms; TR= 1000 ms; ns=2; T. Scan time 2 min 8s). The image resolution is 78 μm . Slice thickness 0.5 mm. (a) eye; (b) brain; (c) gills; (d) heart; (e) swim bladder; (f) intestine; (g) eggs; (h) horizontal myoseptum.

can be excluded if the flow rate of outside water is higher in comparison to the repetition time used for spin echo sequences (23). Furthermore zebrafish cannot tolerate a high flow of water. The experimental time should be kept as short as possible since the zebrafish has a lower tolerance to anesthetic than bigger fish such as carp.

A small flow-through chamber designed to support imaging of living zebrafish is shown in Fig. 2.4A. The chamber was fitted into a cylindrical resonator for a homogeneous excitation profile (Fig. 2.4B). Sagittal and coronal anatomical MR images of living zebrafish were obtained using a RARE pulse sequence with an image resolution of 78 μm (Fig. 2.4C). The flow of water to irrigate the gills of the zebrafish was kept low (20 mL/min) during the measurements. Although the dynamic intensity range of the image was slightly affected by the signal from the surrounding water, sufficient signal-to-noise ratio and image contrast was achieved to distinguish various anatomical details in the images. Several structures such as brain, heart, gills, swim bladder, and intestine can be nicely resolved. The total scan time was 128 seconds. The fish remained under anesthesia in the magnet for up to 15 minutes and recovered uneventfully from the experimental setup. Experiments with live fish were repeated with 5 different animals.

2.4.3 Three-dimensional image reconstruction

In order to emphasize various anatomical structural components and the 3D continuity of these structures, the images are annotated from μ MRI image slices and as a result a 3D model is derived. Figure 2.5 shows a reconstructed three dimensional image of zebrafish obtained from a series of two-dimensional MR slices using TDR-3D base software (25). Here complete three-dimensional models of various structures such as brain, heart, liver, and swim bladder are constructed. While a three-dimensional atlas of zebrafish development produced using TDR-3D base from histological sections is available (18, 26), at this time there is no atlas of the adult zebrafish. We consider this work as a start that will pave the way for

building a high-resolution anatomical atlas of adult zebrafish using both *ex vivo* and *in vivo* μ MRI images.

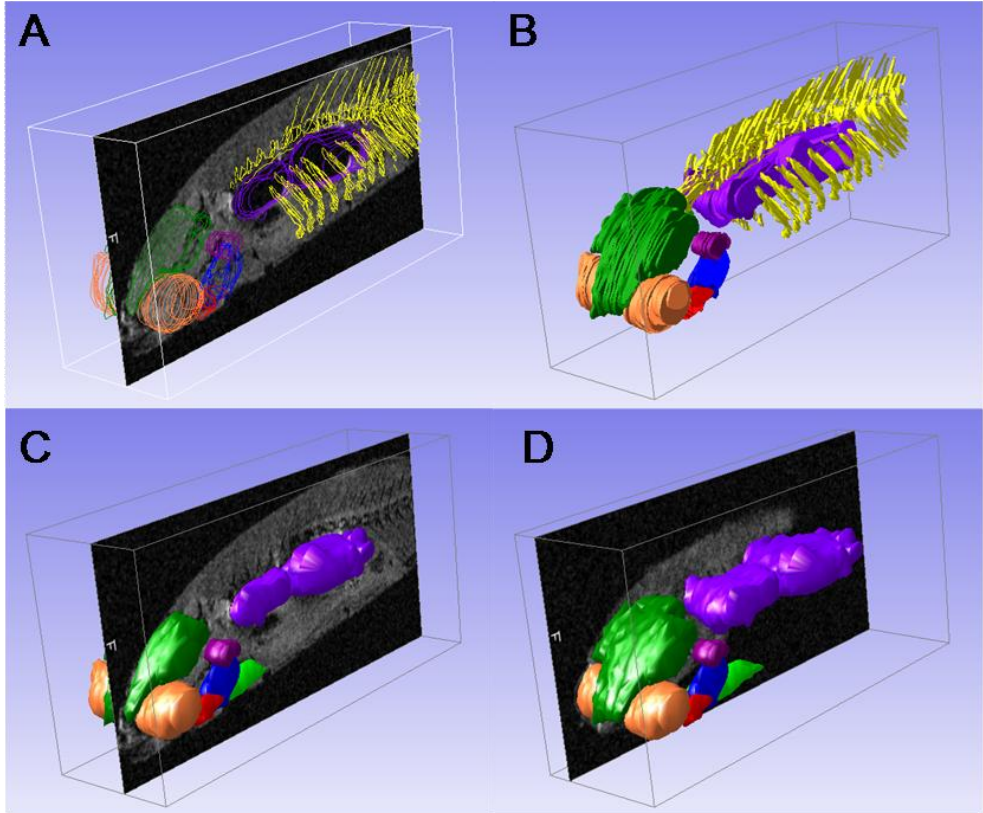


Figure 2.5 3D Visualization of parts of the anatomy of the adult zebrafish reconstructed from 25 MR slices (0.2 mm thick). The slices in the 3D image were annotated with TDR-3Dbase. In panel A the original contours are shown as projected on a slice through the midline of the fish. In panel B the major anatomical structures are visualized as pseudo voxels whereas in panel C and D a surface visualization is shown, projected on a mid-sagittal and lateral sagittal slice. Pleural ribs and vertebral haemal and neural arches (yellow), Brain (green), Swim-bladder (purple), Otic capsule (violet), Eye (salmon), Heart (red), Liver (blue) and Gut (light green).

2.5 Discussion

Zebrafish is rapidly becoming one of the most important vertebrate animal models used in genetic analysis. However, in order to move beyond functional genomic analyses and towards therapies, drugs, and other useful applications, we need to understand the data that these studies generate within the framework of the functional structure of the zebrafish organism in sufficiently intimate detail. Genomics, bioinformatics, proteomics, and other high throughput experimental design paradigms seek to unravel the organism's genetic program by charting its intricately entwined regulatory, sensory, and metabolic pathways, ultimately resulting in a description of life as a system in "information space."

Many such studies analyze correlations of gene expression levels without taking the state of the organism into account. Since the genetic program of an organism is only meaningful in the context of its functional physical structure, imaging is essential to uncover in real space the anatomy that underlies this system of life, its variation between individual organisms with the same or similar genotype, and its structural plasticity under the influence of life processes. Only by understanding the intimate physical structure of life can we gain insight into how the collections of inanimate molecules in living organisms interact with each other to constitute, maintain, and perpetuate the living state—the ultimate goal of life science research (27). For adult zebrafish, profound insight into anatomical and developmental details is missing since analysis with the traditional methods of light microscopy and electron microscopy is difficult, due to distortion, artifacts, and degradation of spatial resolution (3-5). This raises the need for a rapid, sensitive, and noninvasive imaging method such as μ MRI. Our results presented in this chapter show that high field μ MRI provides sufficient

resolution to get rapid anatomical details in adult zebrafish *ex vivo* as well as *in vivo*. Thus high-resolution μ MRI can be applied *in vivo* to study disease development, biological pathways, toxicologic mechanisms, and possible drug screening during various developmental stages in individual living zebrafish noninvasively.

The signal-to-noise ratio of the μ MRI increases linearly with the field strength and since an adult zebrafish is small compared to a mouse or a rat, it would be highly beneficial to further improve resolution by using an ultrahigh magnetic field (7). The optimization of the pulse sequence to image zebrafish at an ultrahigh field of 17.5 T is presently underway.

Acknowledgements

We thank Suzanne Kiihne and Fons Lefeber for technical advice and help concerning the μ MRI and Annemarie Meijer for advice and providing the facility to work with the zebrafish. This work was partly supported by grants from Centre for Medical Systems Biology (CMSB), CYTTRON within the Bsik program (Besluit subsidies investeringen kennisinfrastructuur) and a European Communities 6th framework grant (contract LSHG-CT-2003-503496).

References

1. Van der Sar AM, Appelmelk BJ, Vandenbroucke-Grauls CMJE, Bitter W. A star with stripes: zebrafish as an infection model. *TRENDS in Microbiology* 2004;12:451-457.
2. Langenau DM, Zon LI. The Zebrafish: A new model of T-Cell and thymic development. *Nature Reviews, Immunology* 2005;5:307-317.

3. Poelman RE, Verbout AJ. Computer-aided three-dimensional graphic reconstruction in a radiological and anatomical setting. *Acta Anat* 1987;130:132-136.
4. Verbeek FJ. Theory & practice of 3D-reconstructions from serial sections. In *Image processing, a practical approach*. Baldock RA and Graham J (eds), pp. 153-195, Oxford University Press, Oxford, England, 1999.
5. Louie AY, Huber MM, Ahrens ET, Rothbacher U, Moats R, Jacobs RE, Fraser SE, Meade TJ. *In vivo* visualization of gene expression using magnetic resonance imaging. *Nat. Biotech* 2000;18:321-325.
6. Smith BR, Johnson GA, Groman EV, Linney E. Magnetic resonance microscopy of mouse embryos. *Proc Natl Acad Sci USA* 1994;91:3530-3533.
7. Hogers B, Gross D, Lehmann V, De Groot HJM, Gittenberger-de Groot AC, Poelmann RE. Magnetic resonance microscopy at 17.6-Tesla on chicken embryos *in vitro*. *Journal of Magnetic Resonance Imaging* 2001;14:83-86.
8. Freidlin RZ, Morris HD, Horkay F, Pierpaoli C, Toyama R, Dawid ID, Basser PJ. Diffusion tensor MR microscopy of adult zebrafish. *Proc Intl Soc Mag Reson Med* 2004;11:1755.
9. Smith BR, Linney E, Huff DS, Johnson GA. Magnetic resonance microscopy of embryos. *Com Med Imag Graph* 1996;20:483-490.
10. Bock C, Satoris FJ, Pöter HO. *In vivo* MR spectroscopy and MR imaging on non-anaesthetized marine fish: techniques and first results. *Magnetic Resonance Imaging* 2002;20:165-172.
11. Johnson, GA, Benveniste H, Black RD, Hedlund LW, Maronpot RR, Smith BR. Histology by magnetic resonance microscopy. *Magn Reson Quar* 1993;9: 1-30.
12. Johnson GA, Benveniste H, Engelhardt RT, Qui H, Hedlund, LW. Magnetic resonance microscopy in basic studies of brain structure and function. *Ann N Y Acad Sci* 1997;820:139-148.

13. Maronpot RR, Sills RC, Johnson GA. Application of magnetic resonance microscopy. *Toxicol. Pathol.* 2004;32:42-48.
14. Chatham JC, Blackband SJ. Nuclear magnetic resonance spectroscopy and imaging in animal research. *ILAR J* 2001;42:189-208.
15. Pruitt NL, Underwood SL, Survey W. Bioinquiry making connection in biology. John Wiley and Sons, 2000.
16. Brown MA, Semelka RC. MRI basics principles and applications. John Wiley and Sons, New Jersey, Canada, 2003.
17. Werner M, Chott A, Fabiano A, Battifora H. Effect of formalin tissue fixation and processing on immunohistochemistry. *Am J Surg Pathol* 2000;24:1016-1019.
18. Van der Linden A, Verhoye M, Pörtner HO, Bock C. The strengths of *in vivo* magnetic resonance imaging (MRI) to study environmental adaptational physiology in fish. *Magnetic Resonance Materials in Physics Biology and Medicine* 2004;17:236-248.
19. Mark FC, Bock C, Pörtner HO. Oxygen-limited thermal tolerance in Antarctic fish investigated by MRI and ³¹P-MRS. *Am J Physiol Regul Integr Comp Physiol* 2002;283:R1254-R1262.
20. Bock C, Sartoris FJ, Pörtner HO. *In vivo* MR spectroscopy and MR imaging on non-anaesthetized marine fish: techniques and first results. *Magnetic Resonance Imaging* 2002;20:165-172.
21. Van der Linden A, Verhoye M, Nilsson GE. Does Anoxia induce cell swelling in Carp Brains? *In vivo* MRI measurements in Crucian Carp and Common Carp. *Journal of Neurophysiology* 2001;85:125-133.
22. Verbeek FJ, Huysmans DP, Baeten RWAM, Schoutsen CM, Lamers WH. Design and implementation of a program for 3D-reconstruction from serial sections; a data-driven approach. *Microscopy Research and Technique* 1995;30:496-512.

23. Verbeek FJ, Den Broeder MJ, Boon PJ, Buitendijk B., Doerry E, Van Raaij EJ, Zivkovic D. A standard atlas of zebrafish embryonic development for projection of experimental data. Proc SPIE, Internet Imaging I 2000;3964:242-252.
24. Verbeek FJ, Boon PJ, Sloetjes H, Van der Velde R., Vos N. Visualization of complex data sets over internet: 2D and 3D visualisation of the 3D digital atlas of zebrafish development. Proc SPIE, Internet Imaging III 2002;4672:20-29.
25. Nusslein-Volhard C, Dahm R. Zebrafish: a practical approach. Oxford: University Press, Oxford, England, 2002.
26. Westerfield, M. The zebrafish book. A guide for the laboratory use of zebrafish (*Danio rerio*). 4th ed. University of Oregon Press, Eugene, 2000.
27. Henning J, Nauwerth A, Friedburg H. RARE imaging: a fast imaging method for clinical MR. Magn Reson Med 1986; 3:823-833.

3 *In Vivo* Metabolite Profile of Adult Zebrafish Brain Obtained by High Resolution Localized Magnetic Resonance Spectroscopy*

3.1 Abstract

Zebrafish (*Danio rerio*) is increasingly used as a model organism for understanding brain diseases including neurodegenerative disorders owing to their similar organization of brain components as that of human. However, investigating the brain metabolites of adult zebrafish *in vivo* has not yet been possible. In this study we have implemented and optimized high resolution localized ^1H Magnetic resonance spectroscopy (MRS) at 9.4T and obtained for the first time *in vivo* localized MR spectra from zebrafish brain. High resolution spectra were obtained from a voxel as small as 3.3 μl placed in the middle of the zebrafish brain. Excellent separation of resonances from various metabolites was achieved *in vivo*. In addition, a two dimensional homonuclear correlation spectrum of the zebrafish brain extracts was measured to get a comprehensive metabolic profile of adult zebrafish brain. This study suggests that zebrafish brain has a very similar metabolite profile as the human brain, which proves that zebrafish is a good

*This chapter was published in *J Magn Reson Imaging* 2009; 29:275-281

organism for human brain disorders. Precise *in vivo* biochemical information from distinct regions of the zebrafish brain as obtained in this study can be invaluable for monitoring of disease progression and treatment as well as phenotyping of large number of available zebrafish models of various brain diseases.

3.2 Introduction

Although *in vivo* MR imaging and spectroscopy has become a versatile tool in medicine and pharmacological research (1, 2), very few studies use this method to uncover physiological and biochemical issues in aquatic organisms (3, 4). The zebrafish (*Danio rerio*) is assuming an ever increasing importance as a model for developmental and genetic manipulation studies (5-8). The embryos develop externally and are transparent, facilitating analysis of their development *in vivo*. In addition, the organism can be readily manipulated genetically using either forward or reverse genetic techniques to produce transgenic animals. A large number of zebrafish mutations have been described, many of which phenocopy many human disorders (8). *In vivo* studies of zebrafish are however, mainly restricted to early stages because of the opaqueness of adult phase which cannot be approached by optical imaging methods. Recently *in vivo* μ MRI methods have been optimized to image live adult zebrafish with a 9.4T MRI scanner (9) and sufficient anatomical details from adult zebrafish have been resolved using T_2 weighted fast spin echo sequences.

Zebrafish is also increasingly used as an important model system for understanding the vertebrate central nervous system and brain development (10-12). The basic organization of zebrafish brain is similar to other vertebrate brains (13). The modulatory neurotransmitter system in zebrafish

is highly similar to mammalian systems (14). Considerable knowledge concerning the embryonic development of the brain of zebrafish has accumulated in recent years using optical microscopic imaging methods (15). However, there is an apparent lack of information on the structural organization and neurochemical composition of adult zebrafish brain *in vivo*. While many zebrafish mutants of the central nervous system are available, the molecular mechanism that is operative in many cases is not very well known. The relevance of zebrafish models for human brain diseases should be validated *in vivo*, not only at early embryonic stages but also at adult stage when the brain is fully functional.

The brain metabolites are sensitive to various pathological processes at the molecular or cellular level. For example, N-acetylaspartate (NAA) is believed to be a marker for neuronal number and health, glutamate (Glu) acts as an excitatory neurotransmitter, and myo-inositol (mIns) is thought to be a marker for osmotic stress or astrogliosis (16,17). A comprehensive picture of the metabolites of zebrafish brain is apparently lacking, while neurochemical information of the adult zebrafish brain *in vivo* may be indispensable to follow changes during disease progression at the molecular level. Magnetic resonance spectroscopy (MRS) is one of the few available techniques that, in principle, can provide *in vivo* information on the neurochemistry of zebrafish non-invasively. However, due to the very small size of adult zebrafish brain (5-6 mm), application of MRS in zebrafish will be highly challenging. In addition, being a small aquatic animal, zebrafish requires a special setup and several precautions for supporting *in vivo* MR spectroscopy (9). In the present study we optimized high resolution localized ^1H -MR spectroscopic methods at 9.4T to get for the first time a localized MR spectrum from live zebrafish brain providing metabolite composition of the zebrafish brain *in vivo*. In addition, an

extensive metabolic profile of adult zebrafish was obtained using two dimensional homonuclear correlation spectroscopy of zebrafish brain extracts. The *in vivo* ^1H MRS methods developed in this work for zebrafish brain can be applied in the future to study brain disorders using variety of available zebrafish models for brain diseases.

3.3 Materials and methods

Zebrafisch

Adult wild-type zebrafish (*Danio rerio*) were maintained in recirculating aquarium systems according to established rearing procedures (16). The water temperature was maintained at 28 $^{\circ}\text{C}$ with a flow rate of 150 L/min, with day/night light cycles (12h dark versus 12h light). The fish were fed twice daily with commercial flake food according to Westerfield (16). All fish were handled according to Institutional Animal Care and Use Committee guidelines.

Extraction of the brains metabolites

For extraction of brain metabolites from zebrafish a modified procedure of Suhartono *et al.* (17) has been used. Ten adult zebrafish were euthanized and their brains were carefully removed from the skull and immediately frozen in liquid nitrogen. The brains were crushed in 4 ml methanol and water (1:1). Subsequently 4 ml chloroform was added. The mixture was sonicated for 15 min followed by centrifugation at 5000 rpm at 4 $^{\circ}\text{C}$. After centrifugation two layers were formed: an upper chloroform layer and a lower methanol and water layer (aqueous layer). The two layers were carefully removed and dried under nitrogen flow at 4 $^{\circ}\text{C}$. The dried chloroform layer was dissolved in 1 ml d_4 chloroform and subsequently filtered using Millipore filter. The dried methanol and water layer was

dissolved in 100 mM KD_2PO_4 (pH 6.0) buffer containing 0.02% Trimethylsilylpropionic acid (TSP). This layer is referred to as the aqueous layer in the subsequent sections. Both samples were measured using 1D and 2D ^1H NMR.

Design of a flow-through chamber and experimental setup for in vivo spectroscopy

For *in vivo* $\mu\text{MRI/MRS}$ measurements, a fish was anaesthetised by adding 0.001% MS222 (ethyl meta aminobenzoate metanesulfonic acid salt; Sigma chemical co.) to pH controlled water. Subsequently the fish was transferred to a closed mini-flow-through chamber, which was specially designed to be fitted in a 10 mm volume RF coil to support the living zebrafish inside the magnet (Fig. 1a). The flow-through setup was placed in the centre of the volume coil (1 cm diameter, 4 cm length) (Fig. 1b) inside the microimaging probe, which was then inserted into the bore of the vertical MR magnet (400 MHz). Aerated water with anaesthetic was pumped from a temperature controlled aquarium to a tube entering to the flow-through cell, and opens close to the mouth of the fish. After passing the chamber the water was transported back to the aquarium. The setup allowed direct *in vivo* NMR measurements at constant flow speeds (10 ml/min) which were regulated by a STEPDOS 03/08 pump (KNF Flodos AG, Switzerland). After the MRI/MRS measurements, zebrafish were transferred back to normal aquarium without anaesthetic where fish recovered uneventfully from the experimental treatment within 1-2h.

Magnetic resonance microimaging/ spectroscopy

All measurements were conducted with a 400 MHz (9.4T) vertical bore system, using a transmit/receive birdcage radiofrequency coil with an inner diameter of 10 mm and a 1 Tm^{-1} gradient insert from Bruker Analytic,

Germany. The system was interfaced to a Linux operating system running Topspin 1.5 and Para Vision 4.0 imaging software (Bruker Biospin, Germany).

Localized T_2 - weighted multislice rapid acquisition with relaxation enhancement (RARE) (18) images were acquired to select a volume of interest (voxel). Basic measurement parameters used for the RARE sequence were; echo time (TE) = 15 ms; Repetition time (TR) = 1500 ms; RARE factor = 4. The field of view was 1.0 cm with an image matrix of 256×256 and the slice thickness was 0.2 mm. The MRS voxel ($1.5 \text{ mm} \times 1.5 \text{ mm} \times 1.5 \text{ mm}$) was localized in the centre of the zebrafish brain covering mainly cerebellum and mesencephalon and a small part of diencephalon and medulla. The local field homogeneity was optimized by adjustment of the first and second order shim coil current using the FASTMAP sequence (19). The field homogeneity resulted in a water line width of 20 – 25 Hz.

For 1D localized ^1H NMR spectroscopy, the PRESS (Point Resolved Spectroscopy) sequence was used (20). The sequence consists of 3 hermite RF pulses (90° , 180° , 180°). The TR and TE were 3500 ms and 10 ms respectively. As can be seen in Fig. 1c, the PRESS sequence was preceded by a VAPOR (Variable Pulse Power and Optimized Relaxation Delays) sequence for global water suppression (21) which consists of seven variable power RF pulses with an optimized relaxation delay. Outer volume suppression (OVS) was combined in an interleaved mode with the water suppression scheme, thus improving the localization performance and reducing the demands for spoiler gradients (Fig. 3.1). The OVS scheme used a total of 18 hyperbolic secant RF pulses, each with 90° nominal flip angle and 1 ms pulse length. The PRESS sequence used 2048 complex

points with a spectral width of 10 ppm. The final 1D datasets collected in 256 scans with a scan time of approximately 15 minutes.

Solution NMR measurements

Solution NMR spectra were recorded at 25 °C with a Bruker 400 MHz DMX NMR spectrometer equipped with a pulsed field gradient accessory (Bruker, Germany). 2D homonuclear ^1H - ^1H experiments were performed using the chemical shift correlated spectroscopic sequence (COSY) with a 5 mm inverse triple high resolution probe with actively shielded gradient coils. The ^1H shift was calibrated using TSP as an internal standard. To minimize the relaxation effect and enable reliable metabolite quantification, a repetition time of 3.7s was used during NMR measurements. The concentrations of the various metabolites in the brain extract were determined by comparing the integral peak intensity of the compounds of interest with that of the TSP peak, after correcting for the number of contributing protons and for tissue weight.

Quantification

The acquired *in vivo* spectra were analyzed by using LCModel (22, 23), which calculated the best fit of the experimental spectrum as a linear combination of model spectra. The final analysis is performed in the frequency domain; however, raw data (FIDs) are used as standard data input. The following metabolites were included in the basis set for LCModel: alanine (Ala), aspartate (Asp), creatine (Cr), γ -aminobutyric acid (GABA), glucose (Glc), glutamate (Glu), glutamine (Gln), glycerophosphocholine (GPC), phosphocholine (PCho), *myo*-inositol (Ins), lactate (Lac), N-acetylacetate (NAA), N-acetylaspartylglutamate (NAAG),

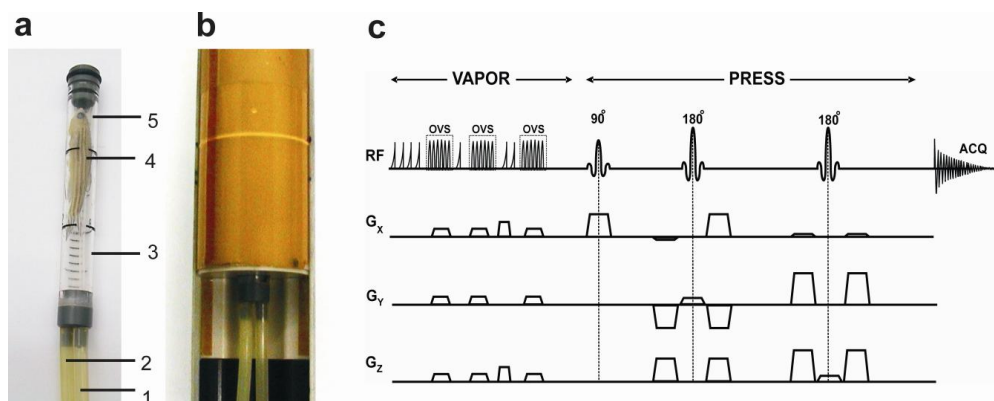


Figure 3.1 (a) Design of flow-through chamber for *in vivo* MRI/MRS measurement of living adult zebrafish. (1) water inlet; (2) water outlet; (3) PVC chamber (inner diameter 8 mm) which holds the fish; (4) a specimen of adult zebrafish; (5) water inlet inside the PVC tube which brings water near the mouth of the fish. (b) Flow-through chamber fitted into the volume coil (10 mm diameter) of the microimaging probe. (c) The PRESS pulse sequence used for localized *in vivo* MR spectroscopy of adult zebrafish brain. The PRESS sequence is preceded by VAPOR sequence for global water suppression interleaved with outer volume suppression (OVS).

phosphocreatine (PCr), phosphoethanolamine (PE), *scyllo*-inositol (sIns), and taurine (Tau). Quantification was obtained by using the tCr resonance as an internal standard. The LCModel fitting was performed over the spectral range from 1.0 to 4.4 ppm.

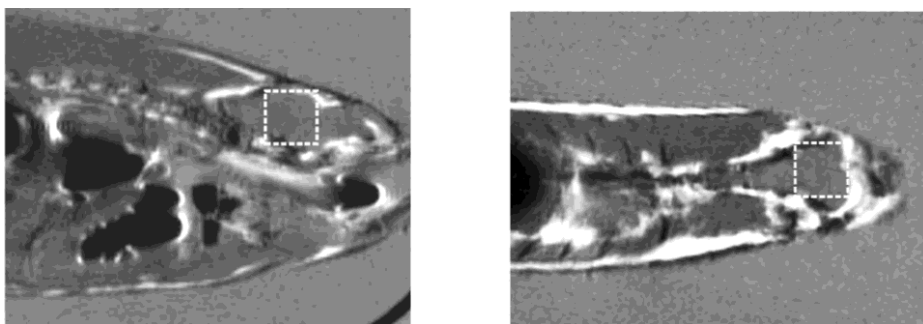
3.4 Results

3.4.1 *In vivo* proton MR spectroscopy of adult zebrafish brain

A small flow-through chamber designed to support imaging of living zebrafish is shown in Fig. 3.1a. This design is adapted from previous *in vivo* studies on zebrafish (9) and was modified so that it can fit into a 1cm RF coil to get high signal-to-noise ratio (SNR) from brain of zebrafish using

μ MRI and MRS. Figure 3.2A shows *in vivo* multislice RARE images of the adult zebrafish brain with a spatial resolution and contrast that guaranteed precise and reproducible placement of the selected volume of interest (voxel) in the center of the brain. Figure 3.2b shows a characteristic *in vivo* ^1H NMR spectrum obtained from the voxel as shown in Fig. 3.2a. Generally short echo time localization methods minimize T_2 relaxation effects, which increases the sensitivity and reliability of metabolite quantification (24). A short echo time of 10 ms was used for *in vivo* 2D MRS in the present study. The spectrum was acquired within 13 min at 9.4T which showed reasonable SNR, resolution and stability. This reasonably good resolution from such a small voxel of only 3.3 μl was accomplished by using FASTMAP automated shimming supported by an efficient shim system (19). In a 3.3 μl voxel, shimming routinely resulted in a unsuppressed water signal line width of 20–25 Hz. Efficient water suppression was achieved using a combination of 7 variable power RF pulses with optimized relaxation delays (Fig. 3.1b). The residual water signal was well below the level of most observable metabolites. Contamination by the signal arising from outside the volume of interest was minimized by outer volume saturation using a series of hyperbolic secant RF pulses, resulting in a sharp volume definition. As can be seen in Fig. 3.2b, in addition to the commonly observed NMR signals of methyl resonances of NAA, tCr, and Cho, characteristic spectral patterns of other metabolites, such as Glu, Gln, Ins and Tau were discernible in the *in vivo* ^1H NMR spectrum from the brain of

(A)



(B)

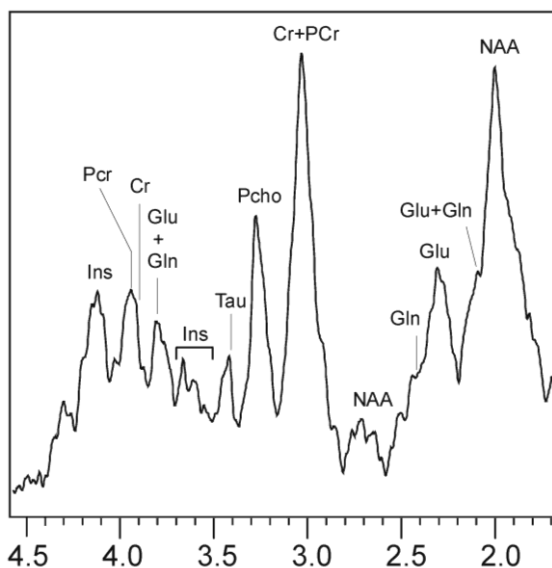


Figure 3.2 *In vivo* high resolution localized MR spectrum from zebrafish brain obtained at 9.4T. (A) MR image in the sagittal and axial planes through the head of living zebrafish, obtained by the RARE sequence with $TR=1500\text{ms}$ and $TE=15\text{ms}$, showing the position of the selected voxel of $3.37\ \mu\text{l}$ ($1.5 \times 1.5 \times 1.5\ \text{mm}^3$) covering most of the brain region. (B) One-dimensional localized MR spectrum from the selected $3.37\ \mu\text{l}$ voxel in the zebrafish brain obtained by the PRESS sequence with $TR=3500\ \text{ms}$ and $TE=15\ \text{ms}$. ^1H -chemical shifts in ppm.

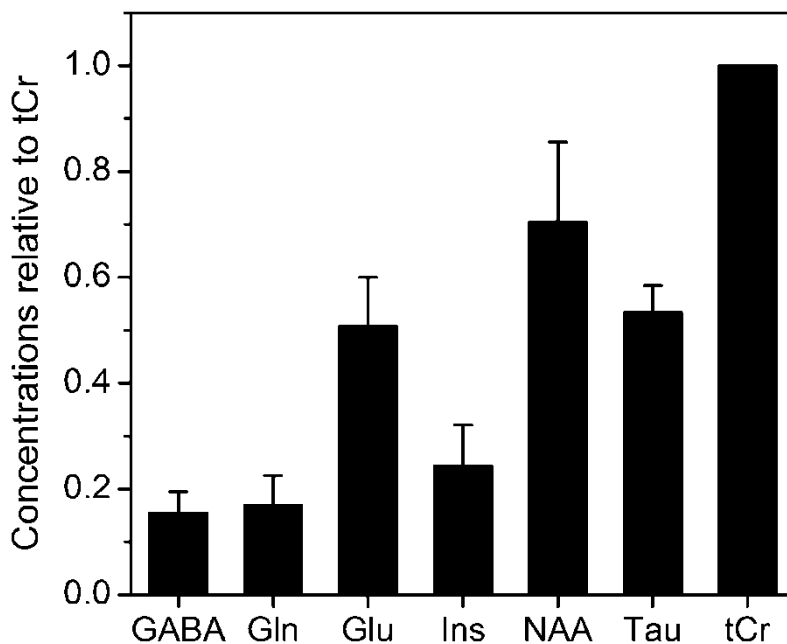


Figure 3.3 Concentrations of metabolites relative to tCr quantified by LCModel in the brain of living zebrafish ($n=4$).

living zebrafish. The *in vivo* ^1H NMR spectrum was analyzed with LCModel to obtain ratios of concentrations of various brain metabolites to tCr. Figure 3.3 shows the concentration of major metabolites in zebrafish brain obtained by LCModel.

3.4.2 *In vitro* proton NMR spectroscopy of the zebrafish brain extracts

To get a wider metabolic profile of zebrafish brain, a 1D ^1H -spectrum has been measured from the extracts of zebrafish brain.

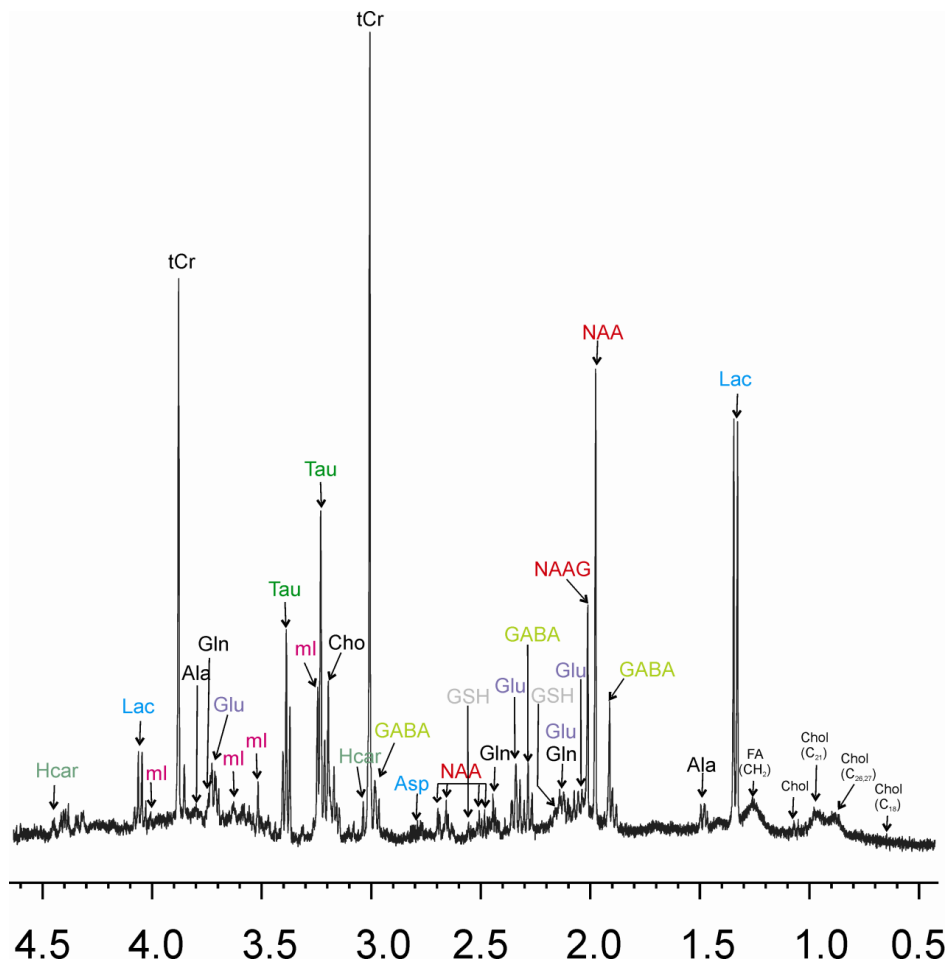


Figure 3.4 High resolution 1D ^1H spectrum of the brain extracts of zebrafish in KD_2PO_4 buffer containing 0.1% TSP. The spectrum was obtained at 25°C with a Bruker 400 MHz DMX NMR spectrometer (Bruker, Germany) using a 5 mm inverse triple high resolution probe with actively shielded two gradient coils. The ^1H shift was calibrated using TPS as an internal standard. Homocarnosine (HCar), lactate (Lac), myo-inositol (mI), total Creatin (tCr), alanine (Ala), glutamine (Gln), glutamate (Glu), taurine (Tau), choline (Cho), gamma-aminobutyric acid (GABA), N-acetyl-DL-aspartic acid (NAA), glutathione (GSH), N-acetylaspartylglutamate (NAAG), fatty acid (FA) and cholesterol (Chol).

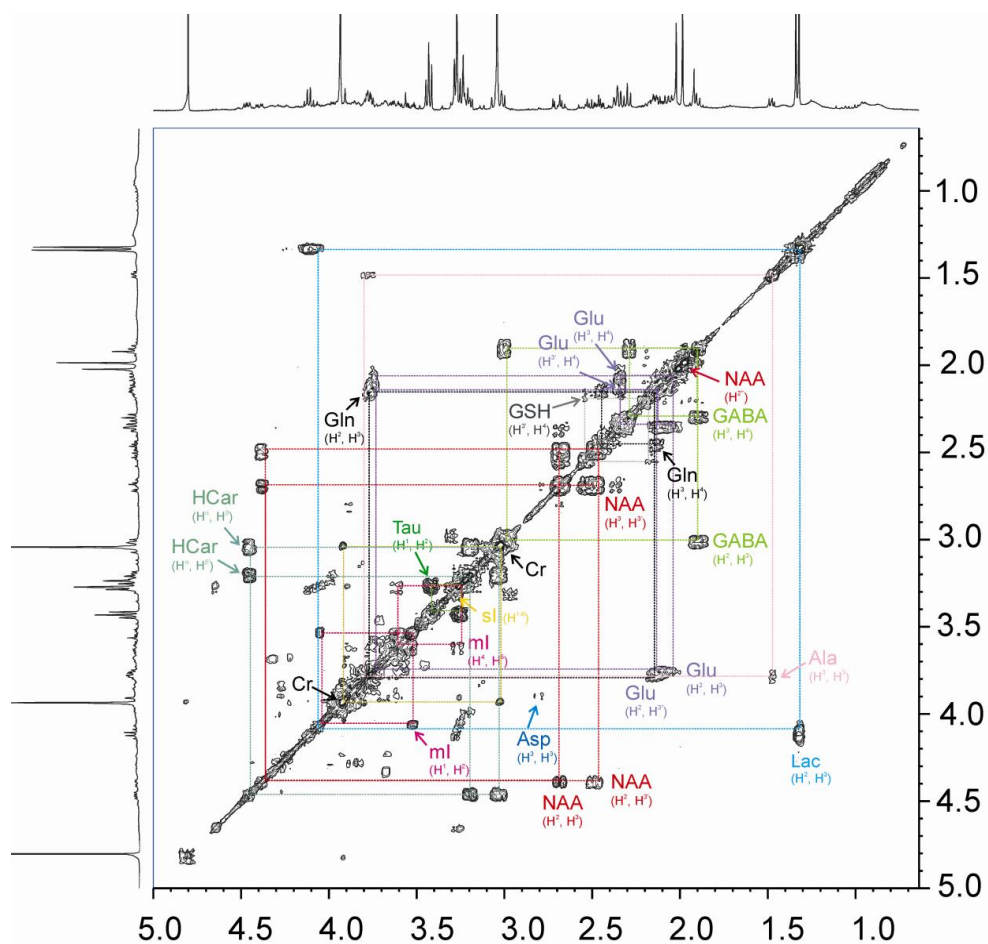


Figure 3.5 High resolution 2D [^1H - ^1H] homonuclear correlation spectrum of the brain extracts of zebrafish obtained at 25°C with a Bruker 400 MHz DMX NMR spectrometer (Bruker, Germany) using a 5 mm inverse triple high resolution probe with an actively shielded two gradient coils. The ^1H shift was calibrated using TPS as an internal standard. ^1H -chemical shifts in ppm.

Figure 3.4 shows the 1D ^1H -spectrum of the aqueous layer of the zebrafish brain extract which was better resolved than *in vivo* spectra and thus allows a more precise assignment of peak identities. In addition to the characteristic metabolites (NAA, Glu, Gln, Tau, tCr and Ins and GABA) that were

recognized in the *in vivo* spectra, many other metabolites such as Lac, Ala, NAAG, homocarnosine (HCar), choline (Cho) and glutathione (GSH), could be reliably measured in the zebrafish brain extracts by 1D ^1H NMR. The one dimensional ^1H spectrum of the brain extracts of zebrafish (Fig. 3.4) shows also a few signals in the lipids region from 0.6 ppm to 1.5 ppm, which were assigned to fatty acids and cholesterol. For the unambiguous assignment of the metabolite resonances in zebrafish brain, a 2D

Table 3.1 The concentrations of various metabolites in the zebrafish brain extracts obtained by ^1H -NMR at 9.4T.

Metabolites	Concentration ($\mu\text{mol/g}$)	Concentration relative to tCr
tCr	8.53 ± 0.25	1.00
GABA	0.89 ± 0.18	0.11 ± 0.02
Gln	1.34 ± 0.15	0.16 ± 0.02
Glu	5.82 ± 1.82	0.68 ± 0.22
ml	2.01 ± 0.26	0.24 ± 0.03
NAA	5.43 ± 1.15	0.64 ± 0.14
NAAG	2.16 ± 0.25	0.25 ± 0.02
Tau	4.59 ± 0.72	0.54 ± 0.08
Ala	0.74 ± 0.09	0.08 ± 0.01
Asp	1.13 ± 0.14	0.13 ± 0.02
Cho	2.60 ± 0.32	0.30 ± 0.31
GSH	1.18 ± 0.29	0.14 ± 0.03
HCar	0.22 ± 0.03	0.03 ± 0.003
Lac	3.70 ± 0.81	0.43 ± 0.09

homonuclear (^1H - ^1H) dipolar correlation NMR spectrum was measured. The 2D homonuclear (^1H - ^1H) NMR spectrum played an important role in the identification, assignment and comparison of resonances of a large number of metabolites in zebrafish brain extracts. The spectrum clearly reveals separate correlation networks of several metabolites. On the basis of cross-peaks a full assignment of several brain metabolites was obtained (Fig. 3.5). Table 3.1 shows the concentration of various metabolites extracted from the brain of adult zebrafish.

3.5 Discussion

Zebrafish is increasingly used as a model organism for understanding brain diseases (5, 6, 14, 25, 26). The zebrafish brain has the same basic organization as other vertebrate brains (13) and there is a complex and well-developed dopaminergic system in the zebrafish (26, 27). Development of quantitative behavioural analysis methods for zebrafish and imaging systems of complete brain neurotransmitter networks at early embryonic stages have enabled comprehensive studies on these neurotransmitter systems in normal and pathological conditions (14). While the early zebrafish developmental stages are likely to be important in the future to analyze brain development and abnormalities produced by gene-knock-out methods, adult zebrafish with a full range of complex brain functions will probably have a significant role in analysis of generally important complex brain functions.

Although the organization of adult zebrafish brain has been studied in detail (10, 13), the metabolic composition of adult zebrafish brain is unknown. The brain metabolites are sensitive indicators of various pathological processes. The *in vivo* assessment of brain metabolites and tracking the

changes in metabolic profile over time will be indispensable tools to understand disease progression and its mechanism. In this study we applied and optimized the ^1H MRS sequence at high magnetic fields of 9.4T to get localized access to the zebrafish brain *in vivo*. Due to the very small size of zebrafish brain, we used an imaging coil of 10 mm to get good signal to noise ratio. To support imaging of living zebrafish, a mini-flow-through chamber was designed that could fit in a 10 mm volume coil (Fig. 1a). The combination of the optimized PRESS sequence, high field strength, strong gradient system, efficient water suppression and the use of short echo time allowed the measurement of high resolution spectra from a voxel as small as 3.3 μl placed in the middle of the zebrafish brain (Fig. 2). Good separation of resonances from various metabolites including NAA, Glu, Gln, Tau, tCr, Ins and PChl was achieved. The relative concentrations of various metabolites relative to tCr in zebrafish brain is shown in Fig. 3.3. The signals are broad when compared to previously reported *in vivo* spectra from various regions in the mouse brain which yield much narrower signals (28). This might be due to eddy currents and/or due to the difficulties in compensating for local magnetic field inhomogeneities in the small zebrafish head as compared to mouse brain.

An extensive metabolite profile and unambiguous resonance assignment of metabolites in zebrafish brain was obtained using the 2D COSY sequence (Fig. 5). The concentration of NAA was slightly lower in the brain extract than in the living zebrafish brain measured by *in vivo* MRS, which might be due to minor degradation during the extraction procedure. The concentrations of other metabolites such as Gln, Glu, mI and Tau in brain extracts were similar to the concentrations obtained *in vivo*. Since regional neurochemical information cannot be obtained in this study due to the small

size of zebrafish brain, a direct comparison of the metabolite profile of zebrafish brain to that of human brain cannot be made. However, in terms of the type of neurometabolites found in zebrafish brain we can conclude that zebrafish brain contains the same basic metabolic composition as found in other vertebrate brains, including human brain.

In conclusion, this study represents the first application of *in vivo* MRS to the zebrafish brain. A flow-through setup has been constructed and the high resolution localized MR pulse sequence has been optimized at 9.4T to get MR access to the small zebrafish brain. A localized MR spectrum from live zebrafish was obtained from a voxel as small as 3.3 μm . The composition of zebrafish brain which was completely unknown so far has been determined in this study for the first time using both *in vivo* and *in vitro* MRS. Future studies with a more advanced pulse sequence, better localization, and use of high magnetic field such as 17.6T may provide access to localized regions in the zebrafish brain. Further development of *in vivo* MRS for zebrafish brain could also include localized ^{31}P and ^{13}C MR spectroscopy which can be important for more extensive analysis of brain changes at the molecular level. The use of *in vivo* localized MRS in combination with μMRI in zebrafish brain can be useful for longitudinal studies to monitor biochemical changes during disease progression and treatment using various available zebrafish models in the near future.

Acknowledgements

We thank Fons Lefeber and Kees Erkelens for technical help concerning the μMRI and Annemarie Meijer for advice and providing the facility to work with the zebrafish. We thank Niels Braakman and Rob van de Ven for the help in using the LCModel data processing program. This work was partly

supported by grants from the Centre for Medical Systems Biology (CMSB) and CYTTRON within the Bsik program (Besluit subsidies investeringen kennisinfrastructuur) and Internationale Stichting Alzheimer Onderzoek (ISAO).

References

1. de Graaf RA. *In vivo* NMR spectroscopy: principles and techniques. 2nd edition. Chichester, West Sussex, England: John Wiley & Sons; 2007. p 43-95.
2. Rudin M, Beckmann N, Porszasz R, Reese T, Bochelen D, Sauter A. *In vivo* magnetic resonance methods in pharmaceutical research: current status and perspectives. *NMR Biomed* 1999;12:69-97.
3. Van der Linden A, Verhoye M, Pörtner HO, Bock C. The strengths of *in vivo* magnetic resonance imaging (MRI) to study environmental adaptational physiology in fish. *Magn Reson Mat Phys Biol Med* 2004;17:236-248.
4. Bock C, Satoris FJ, Pöter HO. *In vivo* MR spectroscopy and MR imaging on non-anaesthetized marine fish: techniques and first results. *Magn Reson Imag* 2002;20:165-172.
5. Bretaud S, Allen C, Ingham PW, Bandmann O. p53-dependent neuronal cell death in a DJ-1-deficit zebrafish model of Parkinson's disease. *J. Neurochem.* 2007;100:1626-1635.
6. Tomasiewics HG, Flaherty DB, Soria JP, Wood JG. Transgenic zebrafish model of neurodegeneration. *J Neurosci Res* 2002;70:734-745.
7. Langenau DM, Zon LI. The Zebrafish: a new model of T-cell and thymic development. *Nat Rev Immunol* 2005;5:307-317.
8. Shin JT, Fishman MC. From Zebrafish to human: modular medical models. *Annu Rev Genomics Hum Genet* 2002;3:311-340.
9. Kabli S, Alia A, Spaink HP, Verbeek FJ, de Groot HJM. Magnetic resonance microscopy of the adult zebrafish. *Zebrafish* 2006;3:431-439.

10. Rupp B, Wullimann MF, Reichert H. The Zebrafish brain: a neuroanatomical comparison with the goldfish. *Anat Embryol* 1996;194:187-203.
11. Giraldez AJ, Cinalli RM, Glasner ME, Enright AJ, Thomsom JM, Baskerville S, Hammond SM, Bartell DP, Schier AF. MicroRNAs regulate brain morphogenesis in zebrafish. *Science* 2005;308:833-838.
12. Jeong JY, Kwon HB, Ahn JC, Kang D, Kwon SH, Park JA, Kim KW. Functional and developmental analysis of the blood-brain barrier in zebrafish. *Brain Res Bull* 2008;75:619-28.
13. Wullimann MF, Rupp B, Reichert H. *Neuroanatomy of the zebrafish brain*. Birkhauser-Verlag, Berlin; 1996. p144.
14. Panula P, Sallinen V, Sundvik M, Kolehmainen J, Torko V, Tittula A, Moshnyakov M, Podlasz P. Modulatory neurotransmitter systems and behavior: towards zebrafish models of neurodegenerative diseases. *Zebrafish* 2006;3:235-247.
15. Kerr JND, Denk W. Imaging *in vivo*: watching the brain in action. *Nat Rev Neurosci* 2008;9:195-205.
16. Westerfield M. *The zebrafish book. A guide for the laboratory use of zebrafish (Danio rerio)*. 4th edition. University of Oregon Press; Eugene; 2000.
17. Suhartono L, Iren FV, de Winter W, Roytrakul S, Choi YH, Verpoorte R. Metabolic comparison cryopreserved and normal cells from *Tabernaemontana divaricata* suspension cultures. *Plant Cell Tissue Organ Culture* 2005; 83:59-66.
18. Henning J, Nauwerth A, Friedburg H. RARE imaging: a fast imaging method for clinical MR. *Magn Reson Med* 1986; 3:823-833.
19. Gruetter R. Automatic, localized *in vivo* adjustment of all first- and second-order shim coils. *Magn Reson Med* 1993;29:804-811.
20. Bottomley PA. PRESS sequence. US Patent, 4 480 228 (1984).
21. Tkac I, Starcuk Z, Choi IY, Gruetter R. *In vivo* ^1H NMR spectroscopy of rat brain at 1 ms echo time. *Magn Reson Med* 1999;41:649-656.

22. Provencher SW. Estimation of metabolite concentrations from localized *in vivo* proton NMR spectra. *Magn Reson Med* 1993;30:672-679.
23. Provencher SW. Automatic quantisation of localized *in vivo* ^1H spectra with LCmodel. *NMR Biomed* 2001;14:260-264.
24. Pfeuffer J, Tkac I, Provencher SW, Gruetter R. Toward an *in vivo* neurochemical profile: quantification of 18 metabolites in short echo-time ^1H NMR spectra of the rat brain. *J Magn Reson* 1999;141:104–120.
25. Campbell WA, Yang H, Zetterberg H, Baulac S, Sears JA, Liu T, Stephen TCW, Zhong TP, Xia W. Zebrafish lacking Alzheimer presenilin enhancer 2 (Pen-2) demonstrate excessive p53-dependent apoptosis and neuronal loss. *J Neurochem*. 2006;96:1423-40.
26. Bai Q, Mullett SJ, Garver JA, Hinkle DA, Burton EA. Zebrafish DJ-1 is evolutionarily conserved and expressed in dopaminergic neurons. *Brain Res*. 2006;1113:33-44.
27. Ma PM, Lopez M. Consistency in the number of dopaminergic paraventricular organ-accompanying neurons in the posterior tuberculum of the zebrafish brain. *Brain Res*. 2003;967:267–272.
28. Tkac I, Henry PG, Andersen P, Keene CD, Low WC, Gruetter R. Highly resolved *in vivo* ^1H NMR spectroscopy of the mouse brain at 9.4 T. *Magn Reson Med* 2004;52:478-484.

4 *In Vivo* Ultra High Field Magnetic Resonance Microimaging to Monitor Malignant Melanoma in Zebrafish

4.1 Abstract

Zebrafish cancer models are fast gaining ground in cancer research. Most tumors in zebrafish develop late in life, when fish are no longer transparent, limiting *in vivo* optical imaging methods. Thus non-invasive imaging of tumor development remains challenging. In this study we applied high resolution magnetic resonance microimaging (μ MRI) to track spontaneous melanomas in stable transgenic zebrafish models expressing a RAS oncoprotein and lacking P53 (*mitf:Ras::mitf:GFP X p53^{-/-}*). Tumors in live zebrafish were visualized at various locations using a T_2 weighted fast spin echo sequence at 9.4T. In addition, live imaging of tumors at ultra-high field (17.6T) revealed significant tumor heterogeneity. This heterogeneity was also confirmed by the significant differences in transverse relaxation time, T_2 measured in various regions of tumor. To our knowledge, this is the first report demonstrating the application of μ MRI to detect the locations, invasion status and characteristics of internal melanomas in zebrafish and suggests that non-invasive μ MRI can be applied for longitudinal studies to track tumor development and real-time assessment of therapeutic effects in zebrafish tumor models.

4.2 Introduction

Zebrafish have emerged as one of the most promising and cost-effective model systems to study cancer susceptibility and carcinogenesis (1, 2). Recent studies have demonstrated that zebrafish cancer has genomic and histological similarities with human cancers, suggesting that experiments in zebrafish cancer models will be highly relevant for clinical studies (3, 4). Genetic screens, transgenic cancer models, and xenograft technologies are providing valuable insights into cancer biology (5).

Advanced melanoma is a devastating and lethal cancer. Significant progress in understanding the basis for this disease has been made (6). Further research, particularly the kind that translates knowledge of the disease into treatment options, will be required to improve the prognosis for melanoma patients. With many tools for studying melanocytes and established melanoma models, the zebrafish is poised to make great contributions toward this goal (7-9). It has been shown that zebrafish melanomas are strikingly similar to their human counterparts (6). Although these studies have been invaluable to demonstrate the potential of zebrafish as a melanoma model, they have been limited by an inability to assess tumor growth and progression *in vivo*. Most of the tumors in zebrafish develop late in life (5, 10, 11). Thus, the lauded advantage of zebrafish embryos being transparent does not apply to most *in vivo* cancer studies in zebrafish that involve adult animals. While a relatively transparent adult zebrafish line that lacks all types of pigments has been generated, it is not applicable to study *e.g.* malignant melanomas that contain melanin pigments. Recently Goessling *et al.* (4) have applied high-resolution ultrasound to follow tumor development and regression by treatment in living adult fish. However, obtaining anatomical details and tumor heterogeneity is beyond the

resolution of ultrasound. Among the many non-invasive imaging techniques available, magnetic resonance imaging (MRI) can provide relatively good spatial resolution and specificity, without ionizing radiation and with limited side effects.

MRI has been widely used to track the presence, development and heterogeneity of various types of tumors in humans as well as in various animal models such as mice, rats etc. (12). However, MRI to detect tumors in adult zebrafish has not yet been explored. Because of their very small size compared to a mouse or a rat, imaging adult zebrafish demands high resolution. Being aquatic animals, zebrafish require a special setup and several precautions for supporting *in vivo* imaging. Recently we have optimized an *in vivo* MR imaging method to image live adult zebrafish using a 9.4 T MRI scanner and obtained for the first time high resolution anatomical details from adult zebrafish using T_2 weighted fast spin echo sequences (13). In addition, MRI in conjunction with MR spectroscopy allowed us to obtain neurochemical composition of live healthy adult zebrafish brain (14).

In this study we used high field Magnetic Resonance Imaging (9.4 T) to characterize the tumor anatomy *in vivo* in a transgenic zebrafish melanoma model (*mitf:Ras::mitf:GFP X p53^{-/-}* fish). This transgenic zebrafish model develops spontaneous melanomas (9). However, the locations and invasion status of melanomas has not been fully studied. The main purpose of this study was to establish parameters for *in vivo* MR microimaging of zebrafish melanomas, to visualize their anatomical locations as well as the extent of invasion. In addition to imaging melanomas in zebrafish at moderately high field (9.4 T), we explored the use of ultrahigh field (17.6 T) to obtain even

better sensitivity and resolution. To obtain detailed information about the heterogeneity of tumors, the proton spin-spin relaxation (T_2) map has been constructed within the tumor volume. Our results demonstrate the feasibility of using μ MRI technique to non-invasively monitor malignant melanomas and their anatomy in living adult zebrafish.

4.3 Materials and methods

Generation of a the transgenic zebrafish model of melanoma

The generation of transgenic zebrafish (mitf:Ras::mitf:GFP X p53^{-/-}) expressing oncogenic human HRasG12V in melanocytes (mitf:Ras::mitf:GFP fish) has been previously described. Stable mitf:Ras::mitf:GFP transgenic fish were crossed with homozygous *tp53*^{M214K} fish to generate mitf:Ras::mitf:GFP X p53^{-/-} fish (10,15).

All wild-type and transgenic zebrafish were maintained in recirculating aquarium systems according to established rearing procedures (16,17). For *ex-vivo* imaging, adult zebrafish were euthanized and immediately embedded in Fomblin (Perfluoropolyether). Alternatively, the fish were fixed in 4% buffered paraformaldehyde (Zinc Formal-Fixx, ThermoShandon, UK) for 2 days and subsequently embedded in Fomblin.

μ MRI

For *in vivo* MRI measurements, a fish was anesthetised by adding 0.001% MS222 (ethyl meta aminobenzoate metanesulfonic acid salt; Sigma chemical co.) to pH controlled water. Subsequently the fish was transferred to a closed mini-flow-through chamber, which was specially designed to be fitted in 10 mm volume RF coil to support living zebrafish inside the

magnet (14). The flow-through setup was then inserted in the centre of the volume coil (1 cm diameter, 4 cm length) inside the microimaging probe, which was then inserted into the bore of the vertical MR magnet (400 MHz). Aerated water with anaesthetic was pumped from a temperature controlled aquarium to a tube entering to the flow-through cell, and opens close to the mouth of the fish. After passing the chamber the water was transported back to the aquarium. The setup allowed direct *in vivo* NMR measurements at constant flow speeds (10 ml/min) which were regulated by a STEPDOS 03/08 pump (KNF Flodos AG, Switzerland). After the MRI/MRS measurements, zebrafish were transferred back to a normal aquarium without anaesthetic where fish recovered uneventfully from the experimental treatment within 1-2h.

MR imaging was performed using a 400 MHz (9.4T) or 750 MHz (17.6T) vertical bore system, using a 10 mm volume coil and a 1 Tm^{-1} gradient insert from Bruker Analytic, Germany. Before each measurement the magnetic field homogeneity was optimized by shimming. Each session of measurements began with a multislice orthogonal gradient-echo sequence for position determination and selection of the desired region for subsequent experiments. For *in vivo* and ex-vivo imaging rapid Acquisition with Relaxation Enhancement (RARE) sequences were used. Basic measurement parameters used for the RARE sequence (18) were echo time (TE) = 15 ms; Repetition time (TR) = 1500 ms; RARE factor = 4. The field of view was 1.0 cm with an image matrix of 256×256 and the slice thickness was 0.2 mm. Data acquisition and processing were performed with Para Vision 3.02pl (Bruker Biospin, Germany) running on a Silicon Graphics 02 workstation with the Irix 6.5.3 operating system and using a Linux pc running XWinNMR 3.2.

For T_2 mapping, a multislice multi echo (MSME) sequence was used. Imaging parameters were: FOV 2.0 x 2.0 cm², matrix size 256 x 256, number of averages 2, number of slices 6 with slice thickness of 0.5 mm, number of echos 8 with TE of 8.5, 17.0, 25.5, 34.0, 42.5, 51.0, 59.5 and 68.0 ms, and a repetition time of 1.5s . For calculation of T_2 relaxation time, regions of interest (ROIs) were drawn at various locations within the tumor. Another ROI in the muscle was used as an internal control. Means and standard deviation for T_2 relaxation times for each ROI were calculated.

Histology and microscopy

Following *in vivo* MR measurements, fish were fixed in 4% paraformaldehyde (Zinc Formal-Fixx, ThermoShandon, UK) at 4°C for 3 days. Fixed fish were decalcified in 0.25M EDTA (pH=8.0) for 4 days, then dehydrated with ethanol and embedded in plastic. Plastic-embedded fish were carefully sectioned (7 μ m) while maintaining the same spatial orientation as in the MR imaging experiments. The sections were stained with toluidine blue and were examined under a Leica MXFLIII stereo microscope and a Zeiss axioplan microscope. Histological images were collected with a digital photo camera (model DKC-5000; Sony, Tokyo, Japan) and produced using Metamorph software (Molecular Devices Corporation, Sunnyvale, CA). Final images were transferred to Adobe (San Jose, CA) Photoshop 7.0 to adjust levels and brightness.

4.4 Results and discussion

Zebrafish are rapidly becoming an accepted organism for cancer modelling. Most of the tumors in zebrafish develop late in life, when the fish is no longer transparent, limiting *in vivo* optical imaging methods. In this study

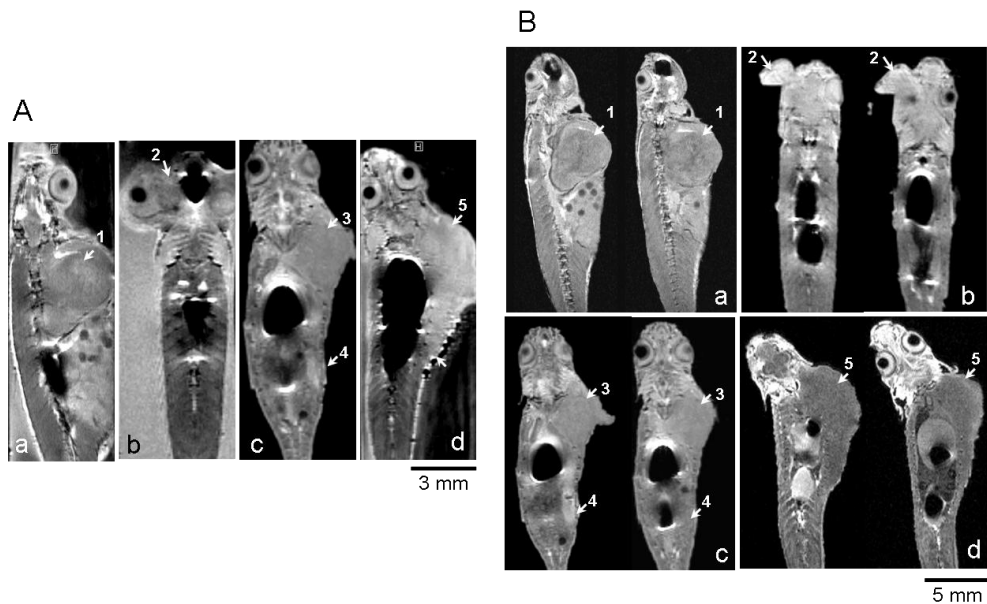


Figure 4.1 Non-invasive detection of malignant tumors in transgenic *mitf:Ras::mitf:GFP X p53^{-/-}* fish zebrafish using high resolution μ MRI. Images of living (A) and freshly killed (B) adult transgenic zebrafish showing presence of tumor at various locations (a-d). (1) malignant tumor seen in: (1) trunk muscles and abdomen that is penetrating into myoseptum and ovary; (2) near eye; (3) back muscles; (4) intestine; (5) back muscle penetrating into liver and intestine .

we applied high resolution μ MRI methods to image internal tumors in live adult zebrafish. Clear morphological proton images were obtained from live fish using the RARE sequence in a short time (4 minutes) (Fig. 4.1). Intermediate signal intensity from the tumor was observed in T_2 weighted images.

Fig. 4.1A shows images of 4 live transgenic zebrafish (a-d) showing tumors at locations such as in trunk muscles and abdomen that is penetrating into the myoseptum and ovary, near the eye, intestine, and liver (Fig. 4.1A).

Fig. 4.1B shows ex-vivo images of the same 4 transgenic fish after they were freshly killed to obtain better image quality. These MR images clearly demonstrate how MRI can provide clear assays of the tumor invasion status in these transgenic fish. To assess the accuracy of *in vivo* MRI in distinguishing tumor type, a three way correlation of tumor bearing zebrafish is shown in Fig. 4.2A(a-c).

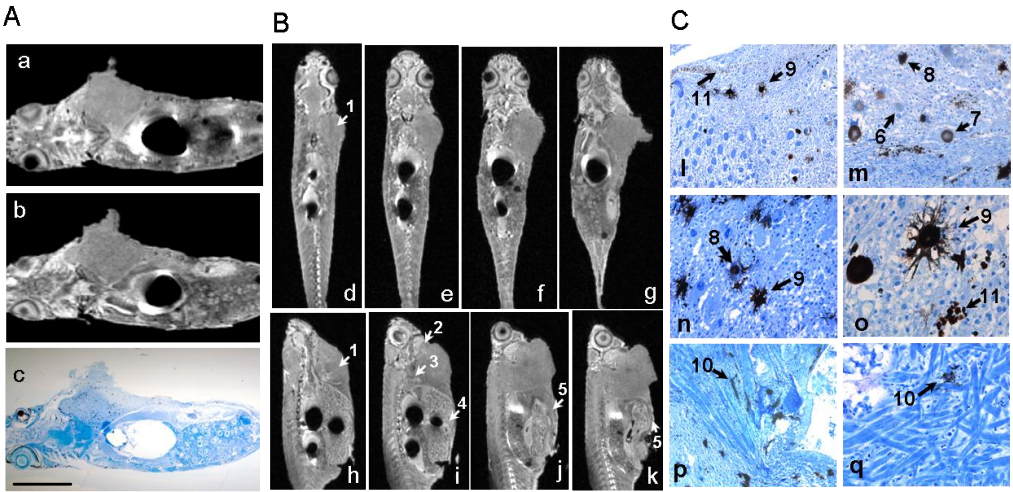


Figure 4.2 Characterization of malignant tumor in transgenic *mitf:Ras::mitf:GFP X p53^{-/-}* zebrafish. (A) Comparison of images of same transgenic zebrafish, with large abdominal tumor, obtained by (a) *in vivo* μ MRI, (b) *ex vivo* μ MRI, and (c) after histological sectioning. (B) Successive μ MRI slices in coronal (d-g) and sagittal (h-k) planes of freshly killed adult transgenic zebrafish showing the abdominal tumor (1) location and its penetration in various organs such as heart (2), liver (3), ovary (4) and intestine (5). (C) High magnification view of a tumor showing its heterogeneity and cell morphology. Different stages of melanocyte differentiation are clearly visible e.g. precursor cells (6) immature (7), mature (8), and dendritic (9) melanocytes. The penetration of melanocytes in muscle cells (10) and melanin vesicles produced by melanocytes (11) are clearly visible. Scale bars (10 mm): 2 mm in (a-c), 5 mm in (d-k), 300 μ m in (l, m, q), 250 μ m in (n, o), 1 mm in (p).

The same transgenic zebrafish with a large abdominal tumor was imaged by *in vivo* MRI, *ex-vivo* MRI and after histological sectioning. An excellent correlation between the tumor visualized by MRI with the histological section was obtained. Fig. 4.2B shows successive slices in coronal (d-g) and sagittal (h-k) planes of a zebrafish with an abdominal tumor showing the location and penetration of the tumor within abdominal regions. The tumor shown in Fig. 4.2Aa-b and Fig. 4.2B was heterogeneous as revealed by histological analysis of the same tumor (Fig. 4.2C). High magnification histological views show the heterogeneity and cell morphology of tumor cells. In addition, the presence of melanocytes and their different developmental stages are clearly detected. Finally, immature, mature and dendritic melanocytes can be seen in this tumor, as well as the penetration of melanocytes in muscle cells and melanin vesicles produced by the melanocytes (Fig. 4.2C). Interestingly, the heterogeneity of the tumor can also be slightly recognized in *in vivo* images, although the tumor appeared more homogeneous in the *ex-vivo* MRI.

To improve the image quality and to clearly probe the heterogeneity of tumor, we explored the use of ultra high magnetic field (17.6T) for μ MRI. Initial experiments were performed to compare the image quality improvement in zebrafish at ultrahigh field. Fig. 4.3 compares the MR image quality obtained from zebrafish head by using moderate (9.4T) and ultra-high field (17.6T) magnetic field strength. The images were collected with same parameter settings at both magnetic fields, to compare image quality rather than shortening the total scan time. The improved image quality was characterized by a better signal-to-noise (SNR), better image contrast, and higher resolution compared to images obtained at 9.4T. As is clear from Fig. 4.3, the brain sub-structures which were not visible at 9.4T

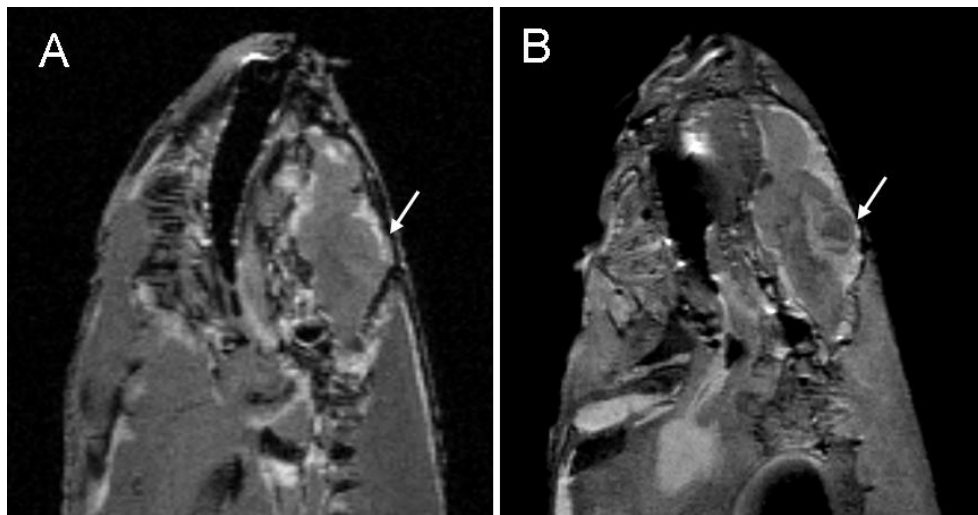


Figure 4.3 High resolution images of adult zebrafish at a magnetic field strength of 9.4 Tesla (A) and 17.6T (B). Slices in the sagittal plane were obtained using the rapid acquisition with relaxation enhancement (RARE) pulse sequence (echo time, 15 ms with effective echo time, 33.6 ms; repetition time, 2000 ms, number of scan, 4, total scan time, 8 min). The image resolution is 78 μm and slice thickness is 0.2 mm. The signal to noise ratio (S/N) at 9.4T and 17.6T was calculated to be 18 and 32, respectively. Image quality improvement is clearly visible at 17.6T, as many substructures in the brain which were not visible at 9.4T, can be clearly seen at 17.6T.

were nicely resolved at 17.6T. At 17.6T, an image with approximately two times better SNR was obtained. The differences between these SNR improvement factors may be due to differences in the saturation of the magnetization and in the T_2 relaxation times in the tissue. The effect of better SNR in resolving structural information at ultra-high field was then applied to visualize tumor anatomy *in vivo*. Fig. 4.4A shows *in vivo* images in the sagittal and coronal planes of the transgenic zebrafish with a lower abdominal tumor. As is clear from this figure, live imaging at ultra high field reveals, that the tumor is highly heterogeneous. The heterogeneity of tumors was also confirmed by the significant differences in transverse

relaxation time, T_2 , measured in various regions of tumor. The spin-spin relaxation time, T_2 , is a specific attribute of spins which depends on their surrounding. Interaction between spins, *e.g.* coupling of neighboring nuclei, destroys the phase coherence and therefore the T_2 relaxation time can be a sensitive indicator of the variation in the microenvironment within a tumor volume. An elevated T_2 relaxation time has been reported within tumors in earlier studies (19). T_2 was also shown to be a sensitive indicator of tumor growth rate¹⁹. We measured the T_2 relaxation time in small regions within and outside the tumor areas as indicated in the MR image inset of Fig. 4.4B. The T_2 was elevated and the T_2 variation within the tumor-bed was quite significant, as can be seen in this figure. The T_2 relaxation times measured in various regions in the tumor ranged between 36.7 ms to 66.3 ms as compared to an average T_2 of 35.9 ms found in healthy muscle tissue outside the tumor. A variety of factors can influence relaxation times within tumor, *e.g.* cellular architecture, regional differences in cellular growth rates, local inflammatory processes (19, 20), necrosis and/or presence of trace amounts of paramagnetic ions or chemical radical species (21). The influence of differences in melanin contents in the tumor cells on T_2 variation cannot be ruled out, although previous studies did not show any clear association between T_2 signal intensity and melanin contents (22). White areas within the tumor-bed correspond to necrotic degenerating mucoid cells which was validated by co-registration of MR images (Fig. 4.5A) with histological sections of the same fish (Fig. 4.5B). The presence of a significant proportion of degenerating or dead cells in addition to numerous proliferating viable cancer cells in rapidly growing tumors is a well known phenomenon.

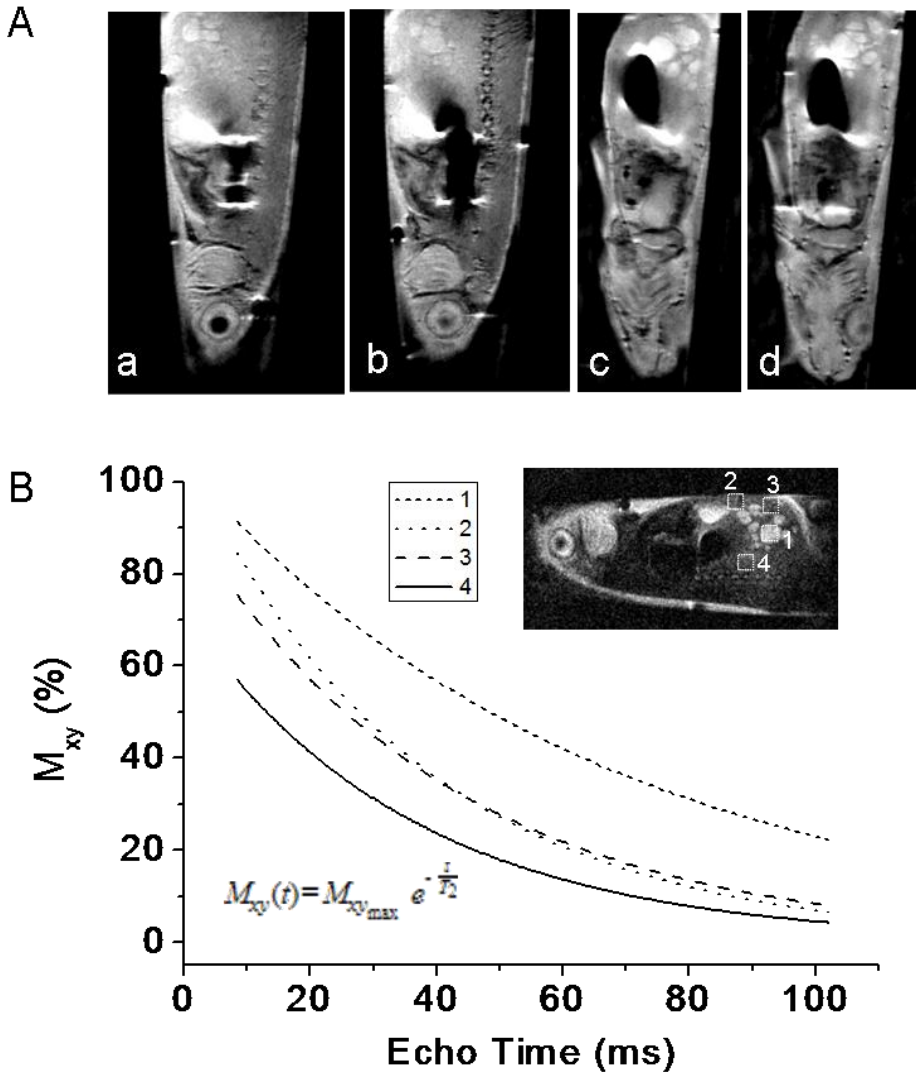


Figure 4.4 *In vivo* characterization of a malignant abdominal tumor in transgenic zebrafish using high resolution *in vivo* μ MRI at 17.6T. (A) μ MRI slices in coronal (a-b) and sagittal (c-d) planes of living transgenic zebrafish clearly showing the heterogeneity of abdominal tumor. (B) T_2 relaxation time measurement of specific regions within (1-3) and outside (4) the tumor as calculated from the plot of echo time (TE) vs T_2 contrast (magnetization present in xy-plane, M_{xy}) by applying the equation as shown at the bottom of the curve. T_2 relaxation times in region 1, 2, 3 and 4 were 66.3 ± 4 , 36.7 ± 2.5 , 42.3 ± 1.3 and 35.9 ± 1.8 ms, respectively.

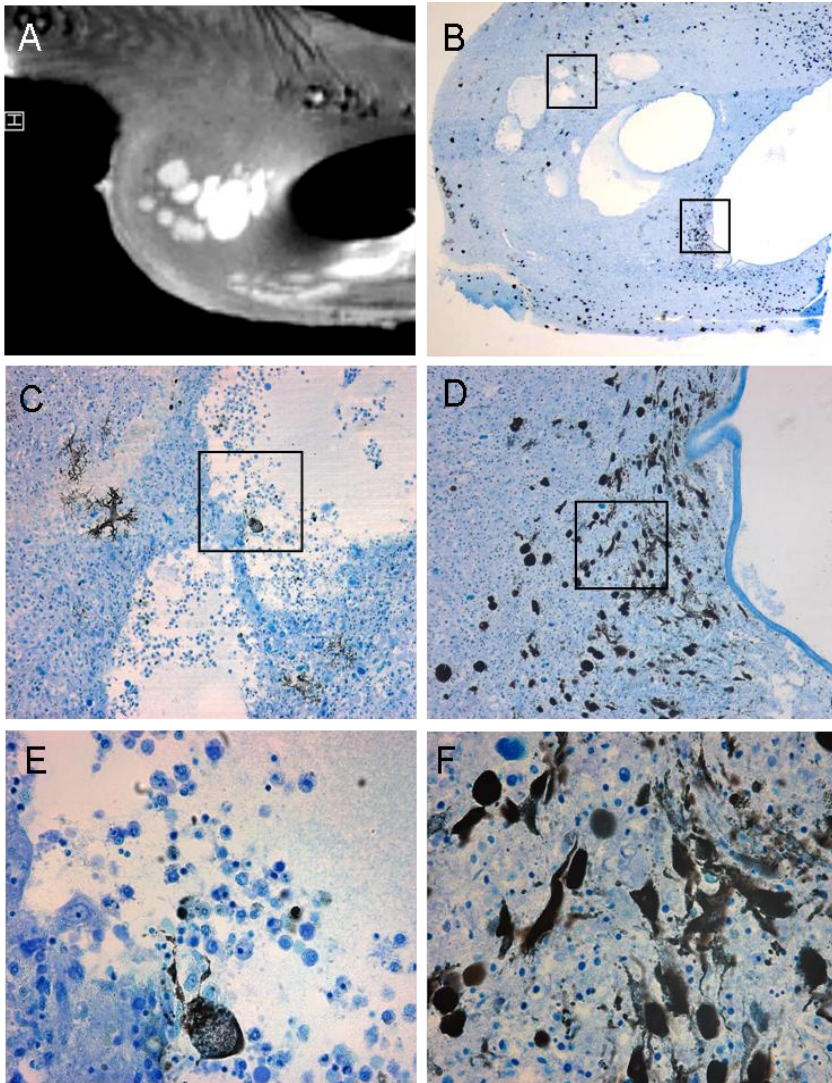


Figure 4.5 Heterogeneity of the malignant abdominal tumor in transgenic zebrafish visualized by (A) high resolution μ MRI at 17.6T and (B) after histological sectioning. C&D are magnified sub-sampled inset of B. E and F are sub-sampled inset of C and D respectively. Scale bars (10 mm): 0.5 mm in (A,B); inset in B $\times 10$ (C,D); inset in C $\times 20$ (E); inset in D $\times 30$ (F).

These dead or dying cells result from incomplete formation of tumor blood vessels and impaired immune cell response. The accumulation of dying cells results in the formation of a dead, or necrotic, core present in virtually all solid tumors. Fig. 4.5 (C & E) shows that these white areas or necrotic cores did not show any well defined borders. In conclusion, our results demonstrate the feasibility of μ MRI technique to detect internal tumors, in live adult zebrafish non-invasively. We have also shown that T_2 relaxation time measurements can provide a means to evaluate the heterogeneity of the malignant tumor. Such non-invasive μ MRI studies may allow longitudinal studies of tumor development and real-time assessment of therapeutic effects in zebrafish tumor models.

Acknowledgements

We thank Fons Lefeber and Kees Erkelens for technical help concerning the μ MRI and Annemarie Meijer for advice and providing the facility to work with the zebrafish. Authors also thank Gerda Lammers for histological sectioning. This work was partly supported by grants from Centre for Medical Systems Biology (CMSB) and CYTTRON within the Bsik program (Besluit subsidies investeringen kennisinfrastructuur). The 750 MHz imaging setup was financed by the Eu grant (BIO4-CT97-2101) and by Bruker.

References

1. Amatruda JF, Shepard JL, Stern HM, Zon LI. Zebrafish as a cancer model system. *Cancer Cell* 2002; 1:229-231.
2. Lam SH, Wu YL, Vega VB, Miller LD, Spitsbergen J, Tong Y, Zhan H, Govindarajan KR, Lee S, Mathavan S, Murthy KRK, Buhler DR, Liu ET,

- Gong Z. Conservation of gene expression signatures between zebrafish and human liver tumors and tumor progression. *Nature Biotechnol* 2006; 24:73-75.
3. Lam SH, Gong Z. Modelling liver cancer using zebrafish: a comparative oncogenomics approach. *Cell Cycle* 2006; 5:573-577.
 4. Goessling W, North TE, Zon LI. Ultrasound biomicroscopy permits *in vivo* characterization of zebrafish liver tumors. *Nat. Methods* 2007; 4:551-553.
 5. Feitsma H, Cuppen E. Zebrafish as a cancer model. *Mol Cancer Res* 2008; 6:685-694.
 6. Ceol CJ, Houvras Y, White RM, Zon LI. Melanoma biology and the promise of zebrafish. *Zebrafish* 2008; 4:247-55.
 7. Patton EE, W. H., Kutok JL, Kopani KR, Amatruda JF, Murphey RD, Berghmans S, Mayhall EA, Traver D, Fletcher CD, Aster JC, Granter SR, Look AT, Lee C, Fisher DE, Zon LI. BRAF mutations are sufficient to promote nevi formation and cooperate with p53 in the genesis of melanoma. *Curr Biol* 2005; 15: 249-254.
 8. Haldi M, Ton C, Seng WL, McGrath P. Human melanoma cells transplanted into zebrafish proliferate, migrate, produce melanin, form masses and stimulate angiogenesis in zebrafish. *Angiogenesis* 2006; 9:139-151.
 9. Michailidou C, Jones M, Walker P, Kamarashev J, Kelly A, Hurlstone AFL. Dissecting the roles of Raf- and P13K-signalling pathways in melanoma formation and progression in a zebrafish model 2009; (in press)
 10. Berghmans S, Zon LI, Look AT. tp53 mutant zebrafish develop malignant peripheral nerve sheath tumors. *Proc Natl Acad Sci USA* 2008; 102:407-412.
 11. Spitsbergen J. Imaging neoplazia in zebrafish. *Nature Methods* 2007;4:548-549.
 12. Cao x, Jia G, Zhang T, Yang M, Wang B, Wassenaar PA, Cheng H, Knopp MV, Sun D. Non-invasive MRI tumor imaging and synergistic anticancer

- effect of HSP90 inhibitor and glycolysis inhibitor in RIP1-Tag2 transgenic pancreatic tumor model. *Cancer Chemother Pharmacol* 2008; 62:985-994.
13. Kabli S, Alia A, Spaink HP, Verbeek FJ, De Groot HJM. Magnetic resonance microscopy of the adult zebrafish. *Zebrafish* 2006; 3:431-439.
 14. Kabli S, Spaink HP, De Groot HJM, Alia A. *In vivo* metabolite profile of adult zebrafish brain obtained by high-resolution localized magnetic resonance spectroscopy. *J Magn Reson Imaging* 2008; 29:275-281.
 15. Thermes V, Grabher C, Ristorator F, Bourrat F, Choulika A, Wittbrodt J, Joly J. I-SceI meganuclease mediates highly efficient transgenesis in fish. *Mech Dev* 2002; 118:91-98.
 16. Nusslein-Volhard C, Dahm R. *Zebrafish: a practical approach*. Oxford: University Press 2002.
 17. Westerfield M. *The zebrafish book. A guide for the laboratory use of zebrafish (Danio rerio)*. 4th ed. Eugene, OR: University of Oregon Press; 2000.
 18. Henning J, Nauerth A, Friedburg H. RARE imaging: a fast imaging method for clinical MR. *Magn Reson Med* 1986; 3:823-833.
 19. Bloch P, Lenkinski RE, Buhle, Jr. EL, Hendrix R, Bryer M, McKenna WG. The use of T_2 distribution to study tumor extent and heterogeneity in head and neck cancer. *Magn Reson Imaging* 1991; 9:205-211.
 20. Kroeker R.M, Stewart C.A, Bronskill M.J, Henkelman, R.M. Continuous distributions of NMR relaxation times applied to tumors before and after therapy with x-rays and cyclophosphamide. *Magn Reson Med* 1988; 6:24-36.
 21. Gore JC, Brown MS, Mizumoto CT, Armitage IM. Influence of glycogen on water proton relaxation times. *Magn Reson Med* 1986; V:463-466.
 22. Premkumar A, Marincola F, Taubenberger J, Chow C, Venzon D, Schwartzentruber D. Metastatic melanoma: correlation of MRI characteristics and histopathology. *Journal of Magn Reson Imag* 1996; 6: 190-194.

5 General discussion and future outlook

The main focus of this thesis was to optimize and apply high resolution MR imaging and spectroscopic methods to obtain the anatomical and molecular information from a living adult zebrafish. The first results are promising and provide basis for applying these methods to monitor disease progression at anatomical and molecular levels using variety of available diseased zebrafish models.

5.1 Future perspectives of MR imaging of the adult zebrafish

One of the areas that stand to benefit from the zebrafish model is the live imaging of anatomical structures and molecular processes in adult zebrafish. Optical imaging studies in zebrafish are restricted to very early developmental stages due to opaqueness of the juvenile and the adult stages (1, 2). Magnetic resonance imaging is a non-invasive modality with exceptional soft tissue contrast. Its non-destructive nature allows a 3D analysis of different tissues in its original environment and the follow-up of the same animals, which is a clear advantage compared to classical histological studies (3, 4). MRI has not yet been applied to image live adult zebrafish. Because of the very small size compared to a mouse or a rat, MR imaging of adult zebrafish needs high resolution. In addition, being an aquatic animal, zebrafish requires special setup and several precautions for supporting *in vivo* imaging (5-7). As shown in chapter 2, we succeeded to

image live zebrafish using μ MRI and obtained for the first time anatomical details from the living zebrafish. This was possible by using high magnetic field of 9.4T in combination with strong magnetic field gradients (1000mT/m) and specialized radio frequency coil (RF) coils. In addition, a 3D model of zebrafish was constructed from μ MRI image slices using TDR-3D base software which allowed complete three-dimensional models of various structures such as brain, heart, liver, and swim bladder are constructed. While a three-dimensional atlas of zebrafish development is produced using the TDR-3D base from the histological sections is available (8, 9), at this time there is no atlas of the living adult zebrafish. We consider this work as a start that will pave the way for building a high-resolution anatomical atlas of adult zebrafish using both *ex vivo* and *in vivo* μ MRI images. The results in chapter 2 demonstrate that high field μ MRI provides sufficient resolution to get rapid anatomical details in adult zebrafish *ex vivo* as well as *in vivo*. In future high-resolution μ MRI can be applied *in vivo* to study disease development, biological pathways, toxicologic mechanisms, and possible drug screening during various developmental stages in individual living zebrafish noninvasively.

It is well known that the signal-to-noise ratio of the MRI increases linearly with the field strength (10). Since an adult zebrafish is small compared to a mouse or a rat, it would be highly beneficial to further improve resolution by moving toward ultrahigh magnetic field. A first attempt to image zebrafish at ultra-high field (17.6T) is presented in Chapter 4. The comparison of the images of zebrafish between ultrahigh high field 9.4 T and 17.6T shows a clear difference in the resolution of the image. The images of 17.6 T were two times better in signal to noise and gave better

anatomical details especially in the brain and the small organs like the heart and the liver. In addition, signal to noise can be further improved by using the cryoprobe technology.

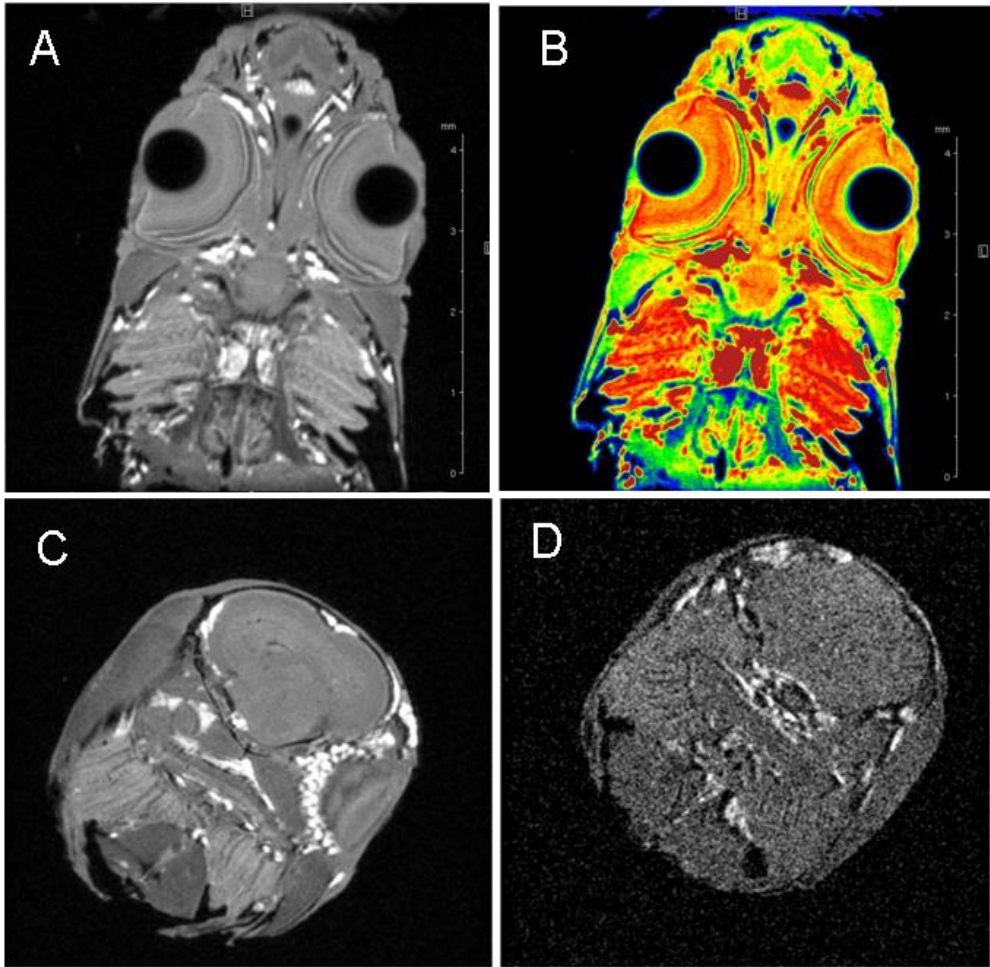


Figure 5.1 Images from the head of adult zebrafish obtained by using micro-imaging cryoprobe (A-C) and conventional Micro2.5 probe (D) at 9.4T with exactly the same experimental data acquisition and processing parameters. Slice in coronal and axial plane were obtained using 3D MSME pulse sequence ($TE= 5.4$ ms; $TR= 1800$ ms; $ns=4$). The image resolution is $43\ \mu\text{m}$.

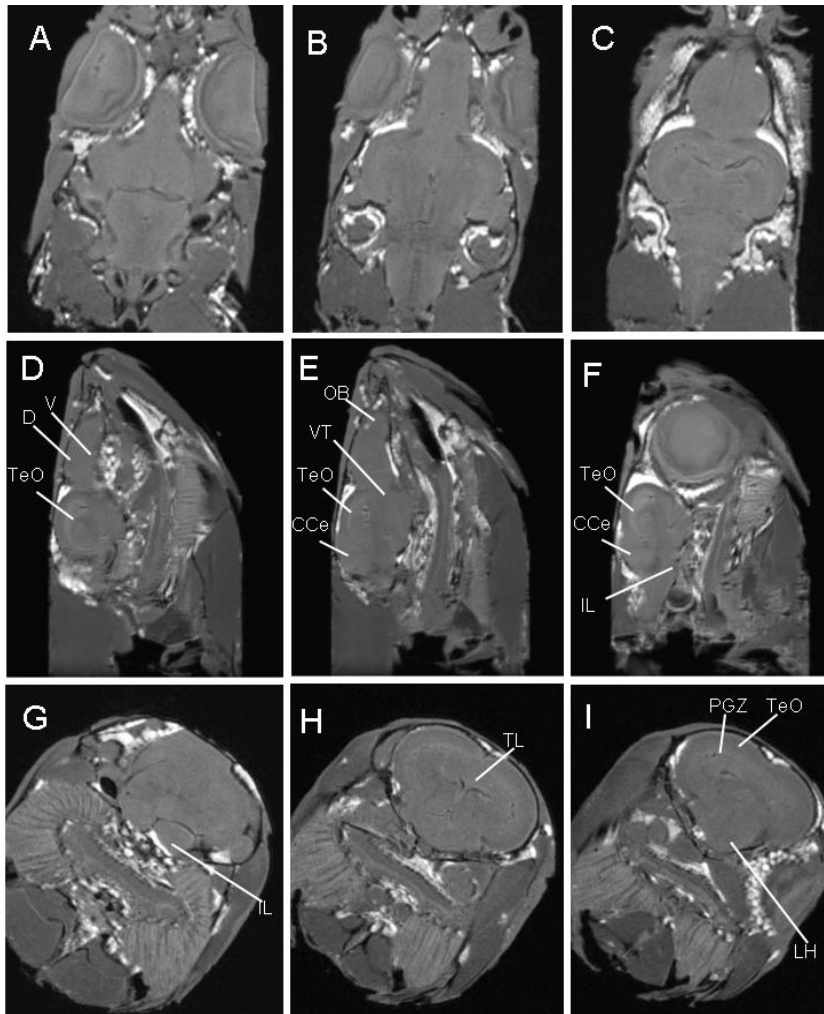


Figure 5.2 Images from the head of adult zebrafish showing anatomical details in the brain obtained by using micro-imaging cryoprobe at 9.4T. Slice in axial plane (A-C), sagittal plane (D-F) and coronal plane (G-I) were obtained using 3D MSME pulse sequence ($TE=5.4$ ms; $TR=1800$ ms; $ns=4$; T ; Scantime 31 min). The image resolution is $43\ \mu\text{m}$. V, ventral telencephalic area; D, dorsal telencephalic area; opticum tectum; OB, olfactory bulb; VT, ventral thalamus; CCe, cerebellar corpus; IL, inferior hypothalamus; TL, longitudinal torus; LH, lateral hypothalamic nucleus

Cryoprobe technology improves signal/noise (S/N) ratios by reducing the operating temperature of the coil and the pre-amplifier. As a result, the efficiency of the coil is improved and the noise of the coil and the pre-amplifier are reduced (11, 12). In a pilot study, we used the cryoprobe in combination with 9.4T to get access to zebrafish anatomy with great details. The cryoprobe was equipped with a ^1H channel for 5 mm diameter samples, an RF coil operated at a temperature of 25 K and an integrated cryogenic preamplifier operated at 77 K. The temperature of the cryogenic probe was fully controlled by the Bruker CryoPlatform. The cooling of the CryoProbes is accomplished with a closed-looped helium gas flow via a flexible transfer line. Using 2D and 3D Multi slice multi echo (MSME) sequence, we observed an increase in the S/N ratio by a factor of 3-4, as compared to images obtained by conventional probe (Fig. 5.1). This improvement in S/N leads to a reduction in experimental time of upto 16. Due to the very small size of zebrafish brain, inadequate S/N ratio can be a major factor limiting the application of μMRI to get anatomical details from the zebrafish brain. As can be seen in Fig. 5.2, several structures within the brain are identifiable including the optic tectum, toris semicircularis, optic ventricle and cerebellum. Improved S/N ratio and possible reduction in experimental time with microimaging cryoprobe will pave the way in the future to follow the zebrafish development from embryo phase till the adulthood non-invasively.

5.2 High resolution localized MR spectroscopy of adult zebrafish brain and future perspective

Due to a similar basic organization of brain components as that of human, zebrafish is increasingly used for understanding brain diseases including neurodegenerative disorders (13, 14). However, there is an apparent lack of

information on the neurochemical composition of adult zebrafish brain *in vivo*.

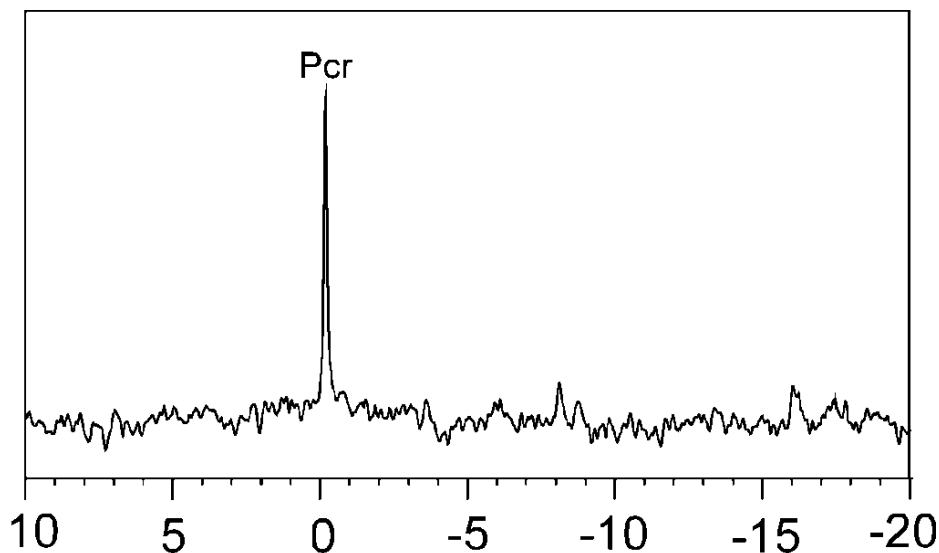


Figure 5.3 *In vivo* high resolution localized ^{31}P MR spectrum from zebrafish brain obtained at 9.4T using ^{31}P _PRESS sequence with TE = 13.45 ms; TR = 1000 ms; Number of averages = 256; spectral width = 5000 hz; scantime = 15 min. ^{31}P chemical shifts in ppm.

In chapter 3, we have successfully optimized a high resolution localized *in vivo* MRS technique to get access to the zebrafish brain and obtained for the first time the neurochemical composition of zebrafish brain. Our results showed that zebrafish brain contains the same basic neurochemical composition as that found in human, suggesting that zebrafish is a good model for studying human brain diseases. Due to the very small size of the zebrafish brain, the regional neurochemical information can not be obtained in this study. Future studies with more advance pulse sequences, better localization and use of high magnetic field such as 17.6T, or use of a

cryoprobe may provide access to localized regions in the zebrafish brain. Further development of *in vivo* MRS for zebrafish brain could also include localized ^{31}P and ^{13}C MR spectroscopy which can be important for more extensive analysis of brain changes at the molecular level (6, 16). In a preliminary experiment, we applied ^{31}P MR spectroscopy to obtain a spectrum from the zebrafish brain.

Due to a small size of the voxel ($3\mu\text{l}$) placed over entire brain, only resonances of phospho-creatine were clearly observed (Fig. 5.3). These results suggest that 9.4 T is not sensitive enough to measure resonances of ATP and P_i in the zebrafish brain. Future experiments at ultra high field 17.6 T may provide better resolution for ^{31}P MR spectroscopy. The use of *in vivo* localized MRS in combination with μMRI in zebrafish brain can be useful for longitudinal studies to monitor biochemical changes during disease progression and treatment using different available zebrafish models in the near future.

5.3 Monitoring spontaneous melanomas in transgenic zebrafish with μMRI and beyond

Zebrafish is emerging as a most promising model system in cancer research. The majority of the tumors in zebrafish develop late in life, when fish are no longer transparent, limiting *in vivo* optical imaging methods (17, 18). Thus *in vivo* imaging of tumor development remains demanding. In Chapter 4, we have successfully applied μMRI to visualize and characterize the tumors in transgenic zebrafish melanoma model at high (9.4T) and ultrahigh (17.6T) magnetic fields. Anatomical locations and invasion status of the tumors were clearly observed. In addition, we have shown that the T_2

relaxation time can provide a means to evaluate the heterogeneity of the malignant tumor (19). Such non-invasive μ MRI studies can be applied in the future, for longitudinal studies to track tumor development or the effects of anti tumor drugs in various available zebrafish tumor models. In addition, if the tumors are homogeneous and solid, it will be easy to apply proton localized spectroscopy to detect the metabolic profile of the tumor and to specifically monitor the changes in the level of choline. It is already known from other studies that many tumors contain high amount of choline than normal tissue (20). In addition to anatomical imaging and localized spectroscopy, MR angiography can be applied to see vascular network in the tumor as well as in other parts of the body (21). It will however be very challenging to apply MR angiography in such a small zebrafish because the vessels are very thin and the water flow outside the fish might influence the signal of flowing blood. Finally, μ MRI can be combined with targeted MRI contrast agents to follow specific processes. For example, *in vivo* visualization of gene expression has been visualized in living *X. laevis* embryos using MRI in combination with contrast agent that can indicate reporter gene expression (22, 23). Use of such contrast agents in combination with *in vivo* μ MRI methods developed in this thesis will be a powerful tool to bridge the gap between the genome wide studies, the morphological, the physiological and the functional studies of the living adult zebrafish.

References

1. Van der Sar AM, Appelmelk BJ, Vandenbroucke-Grauls CMJE, Bitter W. A star with stripes: zebrafish as an infection model. *TRENDS in Microbiology* 2004;12:451-457.

2. Langenau DM, Zon LI. The Zebrafish: A new model of T-Cell and thymic development. *Nature Reviews, Immunology* 2005;5:307-317.
3. Poelman RE, Verbout AJ. Computer-aided three-dimensional graphic reconstruction in a radiological and anatomical setting. *Acta Anat* 1987;130:132-136.
4. Verbeek FJ. Theory & practice of 3D-reconstructions from serial sections. In *Image processing, a practical approach*. Baldock RA and Graham J (eds), pp. 153-195, Oxford University Press, Oxford, England, 1999.
5. Van der Linden A, Verhoye M, Pörtner HO, Bock C. The strengths of *in vivo* magnetic resonance imaging (MRI) to study environmental adaptational physiology in fish. *Magnetic Resonance Materials in Physics Biology and Medicine* 2004;17:236-248.
6. Bock C, Sartoris FJ, Pörtner HO. *In vivo* MR spectroscopy and MR imaging on non-anaesthetized marine fish: techniques and first results. *Magnetic Resonance Imaging* 2002;20:165-172.
7. Van der Linden A, Verhoye M, Nilsson GE. Does Anoxia induce cell swelling in Carp Brains? *In vivo* MRI measurements in Crucian Carp and Common Carp. *Journal of Neurophysiology* 2001;85:125-133.
8. Verbeek FJ, Den Broeder MJ, Boon PJ, Buitendijk B, Doerry E, Van Raaij EJ, Zivkovic D. A standard atlas of zebrafish embryonic development for projection of experimental data. *Proc SPIE, Internet Imaging I* 2000;3964:242-252.
9. Verbeek FJ, Boon PJ, Sloetjes H, Van der Velde R., Vos N. Visualization of complex data sets over internet: 2D and 3D visualisation of the 3D digital atlas of zebrafish development. *Proc SPIE, Internet Imaging III* 2002;4672:20-29.
10. Hogers B, Gross D, Lehmann V, De Groot HJM, Gittenberger-de Groot AC, Poelmann RE. Magnetic resonance microscopy at 17.6-Tesla on chicken embryos *in vitro*. *Journal of Magnetic Resonance Imaging* 2001;14:83-86.

11. Ratering D, Baltes C, Nordmeyer-Massner JA, Marek D, Rudin M. Performance of a 200-MHz cryogenic RF probe designed for MRI and MRS of the murine brain. *Magn Reson in Med* 2008; 59(6):1440-1447.
12. Doty FD, Entzminger G, Kulkarni J, Pamarthy K, Staab JP. RF coil technology for small-animal MRI. *NMR Biomed* 2007; 20: 304-325.
13. Tomasiewicz HG, Flaherty DB, Soria JP, Wood JG. Transgenic zebrafish model of neurodegeneration. *J Neurosci Res* 2002;70:734-745.
14. Panula P, Sallinen V, Sundvik M. Modulatory neurotransmitter systems and behavior: towards zebrafish models of neurodegenerative diseases. *Zebrafish* 2006;3:235-247.
15. Kerr JND, Denk W. Imaging *in vivo*: watching the brain in action. *Nat Rev Neurosci* 2008;9:195-205.
16. Choi JK, Dedeoglu A, Jenkins BG. Application of MRS to mouse models of neurodegenerative illness. *NMR Biomed* 2007; 20: 216–237.
17. Amatruda JF, Shepard JL, Stern HM, Zon LI. Zebrafish as a cancer model system. *Cancer Cell* 2002; 1:229-231.
18. Feitsma H, Cuppen E. Zebrafish as a cancer model. *Mol Cancer Res* 2008; 6:685-694.
19. Ceol CJ, Houvras Y, White RM, Zon LI. Melanoma biology and the promise of zebrafish. *Zebrafish* 2008; 4:247-255.
20. Heerschap A, Jager GJ, Van der Graaf M, Barentsz JO, de la Rosette JJ, Osterhof GO, Ruijter ET, Ruis SH. *In Vivo* Proton MR spectroscopy reveals altered metabolite content in malignant prostate tissue. *AntiCancer Research* 1997; 17:1455-1460.
21. Barrett T, Kobayashi H, Brechbiel M, Choyke PL. Macromolecular MRI contrast agents for imaging tumor angiogenesis. *European Journal of Radiology* 2006; 60: 353–366.
22. Louie AY, Huber MM, Ahrens ET, Rothbacher U, Moats R, Jacobs RE, Fraser SE, Meade TJ. *In vivo* visualization of gene expression using magnetic resonance imaging. *Nat. Biotech* 2000;18:321-325.

23. Stroh A, Faber C, Neuberger T, Lorenz P, Sieland K, Jakob PM, Webb A, Pilgrimm H, Schober R, Pohl EE, Zimmer C. *In vivo* detection limits of magnetically labeled embryonic stem cells in the rat brain using high-field (17.6 T) magnetic resonance imaging. *NeuroImage* 2005; 24:635– 645.

Summary

The zebrafish model combines the relevance of a vertebrate with the scalability of an invertebrate and, in some studies, could provide an interesting intermediate vertebrate model to laboratory small mammals. In addition, the zebrafish genome is available as a preliminary assembly, and numerous mutant lines have been generated. It is clear from the genome studies that practically all disease genes in humans have counterparts in the zebrafish. Among various diseases, zebrafish has also recently entered the stage as a promising model system to study human cancer and neurodegenerative diseases. A better understanding of the comparative anatomy and physiology of adult zebrafish will be required, and *in vivo* imaging methods will be very important to bridge this gap. MRI is an imaging technique that can provide access to adult zebrafish anatomy with good resolution. It has been applied at embryonic stages, but not yet in the adult fish. MRI in conjunction with MRS can be invaluable for studying disease at molecular levels.

This thesis contains the results of imaging of adult zebrafish by using different MR approaches. The relevance of this work is summarized in **Chapter 1**, in addition to a brief introduction of MRI and MRS methods and their relevance to study adult zebrafish.

In **Chapter 2**, we present the first high resolution μ MR images of adult zebrafish. To achieve high resolution we used a magnetic field of 9.4T, in

combination with strong magnetic field gradients (1000 mT/m) and specialized radio frequency coils were used to achieve high spatial resolution. To support imaging of living fish, we designed a special flow-through setup for continuous flow of aerated water to support living zebrafish inside the magnet. Clear morphological proton images were obtained by T_2 -weighted RARE sequences revealing many anatomical details in the entire intact zebrafish *ex vivo* as well as *in vivo*. In addition, a 3D model of zebrafish was annotated from μ MRI image slices which allowed complete three-dimensional models of various structures such as brain, heart, liver, and swim bladder are constructed.

Zebrafish is increasingly used as a model organism for understanding brain diseases; however, there is an apparent lack of information about the metabolic composition of zebrafish brain. It is well known that the brain metabolites are sensitive indicator of various pathological processes. The *in vivo* assessment of brain metabolites and tracking the changes in metabolic profile over time will be indispensable tools to understand disease progression and its mechanism. MR spectroscopy is a non-invasive tool that can be used to measure the chemical composition of zebrafish brain *in vivo*. In **Chapter 3**, we successfully implemented MRS at 9.4T and obtained for the first time detailed composition of zebrafish brain *ex-vivo* as well as *in vivo*. Our results in this chapter suggest that zebrafish brain has similar metabolite profile as the human brain, which proves that zebrafish is a good model organism to study human brain disorders.

Zebrafish models have created their own niche in cancer research. Most of the tumors in zebrafish develop late in life, and the non-invasive imaging tools to detect tumor development in adult zebrafish are lacking. **Chapter 4**

demonstrates the application of high resolution μ MRI methods, which were developed in chapter 2, to track spontaneous tumors in stable transgenic zebrafish models expressing a RAS oncoprotein and lacking P53 (mitf:Ras::mitf:GFP X p53^{-/-}). Tumors were successfully visualized at different locations in live zebrafish. In addition to imaging melanomas in zebrafish at moderately high field (9.4T), we applied ultra-high field (17.6T) to obtain better sensitivity and resolution. Imaging at ultra high field revealed significant tumor heterogeneity which was confirmed by considerable changes in transverse relaxation time, T_2 measured in various regions of tumor. These results demonstrated the feasibility of μ MRI technique to non-invasively monitor tumors and their anatomy in living adult zebrafish. Such non-invasive μ MRI may allow longitudinal studies of tumor development and real-time assessment of therapeutic effects in zebrafish tumor models.

At the end, **chapter 5** provides a general discussion of the work presented in this thesis and a future outlook.

Samenvatting

Het zebravis model combineert de relevantie van een gewerveld dier met de eenvoud van een ongewerveld organisme, wat interessant is voor laboratorium onderzoek. Bovendien is het genoom van de zebravis bekend, en is een groot aantal mutanten beschikbaar. Uit onderzoek is gebleken dat zebravissen en mensen een aantal genen die betrokken zijn bij ziekten, gemeenschappelijk hebben. Recentelijk heeft de zebravis zijn intrede gedaan als een veelbelovend modelsysteem om menselijke kanker en neurodegeneratieve ziekten te bestuderen. Een beter begrip van de vergelijkende anatomie en fysiologie van een volwassen zebravis is nodig en MRI is een beeldvormende techniek die toegang biedt tot de anatomie en fysiologie van een volwassen zebravis met een hoge resolutie. De methode werd eerder toegepast in de embryonale fase, en in mijn proefschrift laat ik zien hoe MRI in combinatie met MRS waardevol kan zijn voor het onderzoek van ziekte op het moleculaire niveau.

In **hoofdstuk 1** wordt de relevantie van het werk samengevat en wordt een korte introductie in de MRI en MRS methoden gegeven, gericht op de studie van een volwassen zebravis.

In **hoofdstuk 2** worden MR beelden van een volwassen zebravis gepresenteerd. De beelden zijn opgenomen in een magneet met een hoog veld van 9.4 T, in combinatie met sterke magnetische veldgradiënten van 1000 mT/m en speciale radiofrequentie (RF) spoelen om een hoge ruimtelijke resolutie in de beelden te krijgen. We hebben ook een opstelling gemaakt voor het continu doorstromen met water om de zebravis levend te houden tijdens de metingen in de magneet. Duidelijke morfologische proton beelden werden verkregen met de T₂-gewogen

RARE spin echo sequenties. Dankzij deze methode werden veel anatomische details in de geheel intacte zebravis onthuld, zowel *ex vivo* als *in vivo*. Tevens was het mogelijk om driedimensionale μ MRI opnamen te maken van organen zoals de hersenen, het hart, de lever, en de zwemblaas.

Bij het onderzoek van hersenaandoeningen wordt de zebravis steeds vaker als model organisme gebruikt. Algemeen wordt aangenomen dat het metabolisme van de hersenen beïnvloed wordt door pathologische processen. De *in vivo* evaluatie van metabolieten in de hersenen en het bijhouden van de veranderingen in het metabolieten profiel gedurende een bepaalde tijd is daarmee een onmisbaar gereedschap om beter de ziekte te kunnen begrijpen. MR spectroscopie is een niet-invasieve meetmethode die gebruikt kan worden voor het karakteriseren van de chemische samenstelling van de hersenen van de zebravis *in vivo*. In **hoofdstuk 3** wordt beschreven hoe we met succes de MRS methode bij 9.4 T hebben geïmplementeerd. Hiermee verkregen we voor de eerste keer gedetailleerde resultaten over de samenstelling van de hersenen van de zebravis, zowel *in vivo* als *ex vivo*. De resultaten van dit hoofdstuk suggereren dat de hersenen van de zebravis een metabolieten profiel hebben dat vergelijkbaar is met het menselijk profiel. Dit bevestigt dat de zebravis een goed model organisme is om menselijke hersenaandoeningen te bestuderen.

Het zebravis model heeft tevens een belangrijke rol in het kankeronderzoek. Het merendeel van de tumoren in de zebravis ontwikkelt laat in het leven van dit organisme. In **hoofdstuk 4** wordt een toepassing van de hoge resolutie μ MRI methoden getoond die in hoofdstuk 2 zijn beschreven. Het doel van deze toepassing is om in een transgeen vis model (mitf:Ras::mitf:GFP X p53^{-/-}) de spontane tumoren te traceren. De tumoren werden met succes gevisualiseerd op verschillende plekken in de levende zebravis. Behalve de resultaten van de afbeelding van melanomen in de zebravis met behulp van de 9.4 T magneet,

werd ook het ultrahoge veld van 17.6 T toegepast om een betere gevoeligheid en resolutie te krijgen in de tumoren. Uit deze metingen blijkt dat de tumoren niet homogeen zijn. Dit werd ook bevestigd door aanzienlijke veranderingen in de transversale relaxatietijd T_2 die gemeten is op verschillende plaatsen in de tumor. Deze resultaten laten zien dat het mogelijk is om in een levende zebra vis de tumoren te bestuderen. Deze niet-invasieve μ MRI resultaten geven de mogelijkheid om in longitudinale studies de groei van een tumor te volgen en ook de effectiviteit van therapeutische middelen te beoordelen.

Ten slotte bevat **hoofdstuk 5** een algemene bespreking van het onderzoek dat gepresenteerd is in dit proefschrift en de toekomstige vooruitzichten.

Curriculum Vitae

In 1993, after finishing my high school education, I started my study at University Hassan II in Casablanca in Morocco at the faculty of natural sciences and mathematics. After 3 years I came back to Amsterdam and in 1997 I started my study in the University of Amsterdam in the faculty of Chemistry. I followed my master internship in the Swammerdam Institute for Life Sciences and the main project was titled “*Determination of the proton affinity of cyclic ethers in the gas phase using the FT ICR Mass spectrometer*” under the supervision of dr. Steen Ingemann. The results were published in the international journal of mass spectrometry. I received my master’s degree in January 2003.

In September 2004, I started my PhD in the solid-state NMR group of prof. dr. H.J.M. de Groot, under the guidance of dr. Alia. During my PhD I had the opportunity to present my work in the form of posters at the 4th *European Zebrafish genetics and development meeting* (2005) in Dresden, Germany, at the *International ISMRM-ESMRMB meeting* (2007) in Berlin, Germany, in the *Genomics Research events* (2007) in Amsterdam, The Netherlands, and at the *First Benelux In Vivo MR Methods Symposium* (2007) in Nijmegen, The Netherlands.

I was invited for oral presentations at the *CYTTRON symposium* (2005) in Leiden, Netherlands, in the *Genomics Research Events* (2007) in Amsterdam, Netherlands, where I was nominated for the seven best projects

for an oral presentation award. Finally I had the opportunity to present my work orally at *the 16th scientific meeting of the International Society for Magnetic Resonance in Medicine (2008)*, in Toronto, Canada.

Since June 2009, I joined the Department of Radiotherapy at the Netherlands Cancer Institute (NKI-AVL), Amsterdam, as a postdoctoral fellow.

List of publications

Full publications

1. Kabli S, Alia A, Spaink HP, Verbeek FJ, De Groot HJM. Magnetic resonance microscopy of the adult zebrafish. *Zebrafish* (2006); 3:431-439.
2. Kabli S, Spaink, HP, De Groot HJM, Alia A. *In vivo* metabolite profile of adult zebrafish brain obtained by high-resolution localized magnetic resonance spectroscopy, *J. Magn. Reson. Imag.* (2009); 29:275-281.
3. Kabli S, He S, Spaink HP, Hurlstone A, Snaar-Jagalska E, de Groot HJM, Alia A. *In vivo* ultra high field magnetic resonance microimaging to monitor malignant melanoma in zebrafish (*submitted*).
4. Bertola LD, Schoonheere E, Wilms I, Kabli S, Alia A, De Groot HJM, Bagowski CP. Effects of hypoxia on buoyancy control and development of lordosis in physostomous and physoclistous fish species. (*submitted*).

Conference proceedings

1. Kabli S, Spaink HP, de Groot HJM, Verbeek FJ, Alia A. *In vivo* magnetic resonance microimaging in adult zebrafish. *Proc. Intl. Soc. Mag. Reson. Med.* 2007; 15: 1347.

2. Alia A, Kabli S, Gross D, Marek D, Oerther T, Sacher M, Spaink HP, de Groot HJM. Magnetic resonance microimaging of adult zebrafish brain using cryoprobe technology. *Proc. Intl. Soc. Mag. Reson. Med.* 2007; 15: 1056.

3. Kabli S, Spaink HP, de Groot HJM, Alia A. *In Vivo* High resolution Magnetic Resonance Spectroscopy of the Adult Zebrafish Brain at 9.4T. *Proc. Intl. Soc. Mag. Reson. Med.* 2008; 16: 113.

Nawoord

Amsterdam, Juni 2009

Vandaag wil ik graag iedereen bedanken die op één of andere manier heeft geholpen bij de uitvoering van mijn project en/of heeft bijgedragen aan de plezierige omstandigheden waarin ik de afgelopen jaren aan mijn project heb gewerkt.

In de eerste plaats wil ik mijn promotor Huub en co-promotor Alia, bedanken. Met hen heb ik van het begin tot het einde regelmatig overlegd in een plezierige sfeer. Hun advies, steun en het vertrouwen in mij en mijn project, hun feedback, tijd en hulp hebben ertoe geleid dat mijn project aangenaam is verlopen. Tevens hebben ze een belangrijke bijdrage geleverd aan het resultaat. Ik kijk dan ook met plezier terug op onze samenwerking. Daarnaast wil ik ook Herman Spaink bedanken voor de steun die hij mij gaf met zijn expertise. Annemarie Meijer die me heeft geleerd met de ethiek en de techniek om te gaan van de vissen om te gaan. Christoph Bagowski voor het opofferen van wat grotere zebravissen in het begin en voor het optimaliseren van de MRI sequencies. Ik wil ook Fons, Johan en Kees bedanken voor de goede steun bij alle technische complicaties in NMR apparaten. Liesbeth de (big sister) van de groep en Wim voor alle koffiepauzen. Bianca en Louise, bedankt! voor de usersmeetings. Die

meetings hebben me geholpen om mijn MRI kennis te verbreden. Ik wil ook Fons Verbeek bedanken, samen met hem heb ik het eerste 3D model van de zebravis gemodelleerd en hierdoor heb ik de anatomie van het visje goed leren kennen. En ik wil natuurlijk Niels bedanken voor de steun, de discussies en het gezelschap tijdens de conferenties. De leescommissie bedankt!

I would like very much to thank all my international colleagues as well, thanks a lot for the nice time we spend together! Thank you Piotr for the activities and AIO meetings, thank you Firat, Anjali, Swapna, Anna, Esha and Prashant for the lovely conversations we had during the lunch breaks! Eugenio, thank you for the cosy discussion about politics! Thanks both Robs, Reijnier, Joerg, Francesesco, Khuram, Geertje, Smitha and Thierry for the nice work atmosphere! My great thanks to Karthik for keeping an eye on my fishes and feeding them during weekends. Thanks a lot Shuning and Adam from the Manchester group for your collaboration during my work on the cancer study! Marzena, great thanks to you for helping me with the printing of the thesis, and my paranimphs! Thanks a lot for the defense day!

Verder wil ik in dit verband mijn vrienden bedanken vooral Ahmed, Elias, Fatiha, Najlae, Yaming, Olga en Mounia (via haar heb ik dit project gevonden). Ik wil ook mijn zusjes Nawal en Souad en mijn broertjes Youssef en Zakaria bedanken voor hun praktische en morele steun tijdens dit project.

En tot slot wil ik mijn ouders bedanken voor de gelegenheid die ze mij hebben gegeven om mijn eigen weg te vinden. Evenals, ma grand-mère,

merci pour tous et surtout pour la discipline que tu m'appris quand j'étais petite.

